Cell Microscopy Imaging:
A Review on Digital Image Processing Applications

Rubén Orozco Morales and Juan Valentín Lorenzo Ginori

Abstract

The great advances in digital technology as well as in the light microscopy field in recent years, determined that digital cellular imaging had acquired a growing importance in cell biology. New and more sophisticated acquisition methods, like those employed in high content screening, usually produce a huge amount of data which demands the power of computers to analyze them. This approach not only allows increasing speed but also can supersede some limitations inherent to human observers. Computer image analysis in cell microscopy can address diverse tasks like (among others) cell classification and counting, studies on sub-cellular structures and studies on living cells. It also targets fields like pathology, vegetable bio-technology, toxicology, drug development and others.

This work reviews a selection of the most updated literature related to digital image processing in cell imaging. Topics covered begin with image restoration with functions like correcting uneven illumination, noise filtering and reduction of blurring. Then image segmentation especially oriented to cell images is addressed, including the separation of cell aggregates and how to evaluate the segmentation effectiveness and compare the algorithms' performance for specific tasks. Finally, some pattern recognition and classification issues in cell image processing are considered. It is the author's hope that this review article will help the researchers in this field to have a rapid orientation, which can make easier for them to develop or select an appropriate algorithm, suited to the needs of the cell image processing problem to be solved.

Keywords: Cellular imaging, digital image processing.

1. INTRODUCTION

Automated analysis of diverse information related to biological structures and functions of living organisms has become a remarkable area in biological research, in which images are one of the most relevant classes of related data. Due to the great advances in the digital technology as well as in the light microscopy field during the past two decades [1], the studies on cell biology through cellular imaging have acquired a

[1]continuously growing importance. The computational tools developed so far allow performing molecular imaging at the cellular and molecular level and has been recognized as a main area of research and development in Digital Image Processing (DIP) [2]-[4]. In particular, remarkable developments that have contributed to this growth are fluorescent probes and high resolution microscopes. The role of cell microscopy in research related to genome and proteome has gained a primary significance, which includes studies on living cells, such as cell phase identification, cell tracking, or tracking of sub-cellular structures. New and more sophisticated acquisition methods are being developed, that usually produce a huge amount of data which demands the power of computers in order to analyze them. The area of high content screening [5], [6] is an example of this situation, for which some examples will be presented in the section on current applications.

Computer image analysis in cell microscopy also targets fields like pathology, vegetable bio-technology, toxicology, drug development and others. There exist various examples of software systems that have been developed for cell image analysis, among them [7]-[10]. The importance of open source code in bioimage informatics for cell biology applications is stressed in [11].

This article deals with the digital image processing issues related to cellular bio-imaging. Digital image processing is a wide field for which an excellent treatment can be found in [12]. DIP comprehends numerous applications; see for example [14], [15]. In the particular case of cellular imaging, DIP applications can encompass also image analysis and pattern recognition tasks, which fall in the general field of computer vision. The objective there is to substitute the human experts in analyzing cell images, in order to obtain useful information about diverse biological processes. There are several motivations for doing this: analyzing great amounts of microscopy images by human experts tends to be a tedious and time-consuming task, which is prone to intra- and inter-analysts errors due to tiredness and subjectivity. There are also limitations of the human visual system (like the limited number of gray levels or colors that can be discriminated) that can be superseded by the computer image analysis systems. The

_____

[1]

current (and ever growing) speed of computers is also a key factor that strongly influences the productiveness of the automated cell image analysis systems, with extensive use of digital image processing.

Digital image processing systems for cellular imaging applications involve many of the standard functions that are found in general DIP systems, but that are specifically configured to cope with many task specific issues. In this case, selecting or developing and implementing an appropriate algorithm for cellular imaging applications is strongly influenced by the characteristics of the microscopy technique used and also by the nature of the images to be processed.

There are currently a variety of optical microscopy modalities that can be employed for cell imaging: brightfield, darkfield, phase contrast, polarization contrast, differential interference contrast, widefield fluorescence and confocal laser scanning fluorescence, as described in [1]. On the other hand, there are a huge variety of different cells from living organisms, whose images can be very different in regard of many attributes. This means that there are not general solutions for cell image processing: instead the algorithms are to be devised according to the characteristics of each class of images. This diversity can be appreciated in the examples of Figure 1, where four different cell microscopy images are shown.
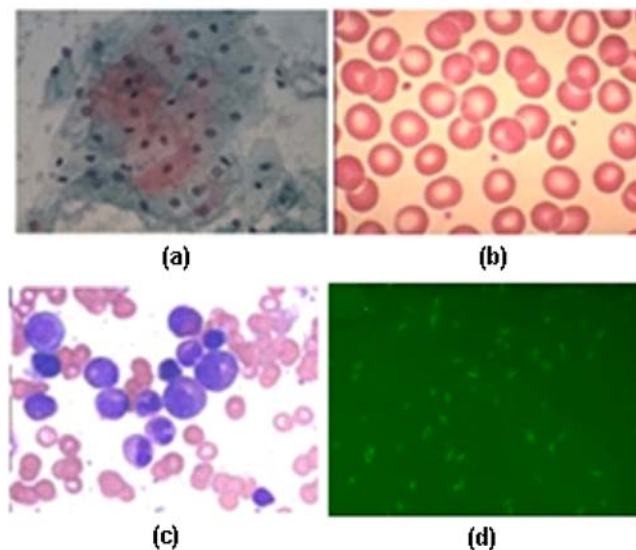

(a)　　　　(b)

(c)　　　　(d)

Fig. (1). Examples of cell images, (a) cervical cytology image, (b) human peripheral blood smear, (c) bone marrow, (d) fluorescence microscopy image of *e-coli*. Actual colors are very diverse.

The main applications to be addressed in this article are organized in the sections described in the next paragraphs, and throughout the paper it will be assumed that the reader has at least an introductory knowledge of the basic topics related to DIP.

Image restoration is understood as the set of techniques used to improve the image quality before performing further processing. This topic is addressed in a first section, discussing non-uniform illumination correction, image deblurring and noise filtering.

Following this section the problem of cell image segmentation is addressed. It is to be stressed the fact that a universal segmentation method which can exhibit the best performance in every situation does not exist. In this paper, the most widely employed methods for cell segmentation like watershed transform and level sets are presented, and some others are briefly summarized. An important issue discussed here is segmentation of touching or overlapping cells that must be separated in order to analyze the cells individually. As a last important issue on segmentation, some techniques to evaluate and compare the performance of different algorithms are presented.

The whole process ends with data analysis, which usually includes statistical modeling and image classification; this is addressed in the next section. Data analysis is more on the side of computer vision, and although it is somewhat beyond the scope of the strict image processing field, is briefly presented here. Finally, a last section is devoted to show and make a short discussion of some specific applications in which many of the DIP processes analyzed in the previous sections are combined to solve the problems inherent to them.

The algorithmic implementation of the functions that are necessary to perform a cell DIP task is usually realized the in form of a pipeline, as illustrated in Figure 2, where image restoration includes illumination correction, deblurring and denoising.

According to the previous paragraphs, DIP techniques used in cellular imaging are very diverse and are usually selected and applied in order to satisfy the needs of

specific situations. Having in mind that in the last years there have been published hundreds of articles in this field, the authors have attempted to make a meaningful selection of significant papers, with the hope that reviewing them will provide a comprehensive overview of the state of the art in the field, as well as introducing the beginners to the most used techniques. This hopefully will help to have a rapid orientation when addressing a specific problem, as well as appropriately selecting or developing the algorithms needed for the cell image processing problem under study.

Fig. (2). Algorithmic pipeline for cell image processing.

2. IMAGE RESTORATION

Under the general term "image restoration", the DIP operations related to non-uniform illumination correction, denoising and deblurring will be considered in this section. It is to be recognized, however, that there are other image processing functions that can be potentially employed in the image restoration stage, as it is the case of interpolation [16] or superresolution [17], which we will not consider explicitly in this article because these have not found an expression yet in the literature on cell image processing reviewed in this article. Before discussing techniques to improve the image quality prior to further processing, it is worth noting that there have been published work specifically devoted to evaluate the image quality. For example, in applications like high content screening, images of too poor quality should be detected and discarded, because they might decrease the accuracy and reproducibility of routines such as cell counting and may lead to meaningless results. The problem of quality evaluation of fluorescence images was addressed in [19], paying attention to separation of objects and background and allowing the evaluation of the suitability of the images for an automated analysis by means of some parameters. An approach to quality evaluation based in artificial neural networks was introduced in [20].

2.1. Non-uniform illumination correction

Illumination in microscopy images often has a noticeable fluctuation that can be more than 1.5-fold across the field of view, even if fiber optics light sources are used, and sometimes including cases where commercial illumination-correction from image analysis software is employed. Non-uniform illumination implies the existence of an illumination gradient and this means that the background does not have the same intensity at all pixel locations except for random noise, affecting the intensity level in the positions where the cells are located.

This effect prevents an appropriate segmentation of the image and can deteriorate the overall behavior of any computer vision system for cell analysis. Correction of shading in the microscope using the flat-field technique [1] can be employed to solve this problem, however a new empty field is needed whenever the microscope illumination setting is modified, which means a tedious and time-consuming task, not tolerable in cases like high throughput imaging systems, where very short acquisition time is needed due to the large number of images to be captured and processed. For this reason, image processing techniques are preferred in this case to correct the non-uniform illumination. Correcting the non-uniform illumination using an appropriate algorithm can be thought in general as determining the varying background intensity and subtracting it from the original image. Some recent works that deal with the correction of this impairment will be analyzed, with emphasis in the illumination correction method based in grayscale mathematical morphology.

A non-even illumination correction method based in the estimation of the background illumination level and its subtraction from the image was introduced in [20], [21], in the context of high-throughput image-based siRNA screens of mammalian cells. In this case the background estimation was made by means of a low-pass filter with a kernel at least twice the diameter of the cell nuclei. This produced a blurred image that when subtracted from the original image, reduced the grey levels of the background while the objects of interest remained at a significantly higher intensity. After this, further local background correction was made. A second example of using non-uniform illumination correction techniques can be found in [22] in the context of the detection and counting of "in vivo" cells to predict cell's migratory potential. In this case,

the background is considered as a varying mean value of an illumination gradient. This varying mean was approximated by a surface calculated through mean filtering with a large window. As a result, the filtering surface obtained is what would result if all the local variations in the illumination (due to objects like cells, or to random noise) were ignored. In a last step, the obtained 2D background function is subtracted from the original image, producing the desired correction.

Another example is described in [23], which consists in applying a regional maxima kernel (equivalent to a grayscale morphological dilation) to the image, in order to separate the bright pixels from the dark ones. However, the authors recognize that this process modifies the grayscale values and that this can affect the intensity values.

The morphological grayscale top-hat operation can be used in general situations for correcting the uneven illumination. The basic morphological gray-scale operations in which this technique is based are described in detail in [24]. Given a grayscale image f and a structuring element (SE) B (another set of a determined shape, that will be considered flat here) the grayscale morphological top-hat transform of a grayscale image f is given by

$$f \circ \hat{} B = f - (f \circ B), \tag{1}$$

where $\hat{o}$ denotes the open top-hat operation and $\circ$ the morphological opening. This transform, when the size and shape of the SE are appropriately chosen, can be used very effectively to correct the non-uniform illumination. This principle was applied in the analysis of fluorescence microscopy images of e-coli cells in [25]. The morphological top-hat approach preserves the illumination level of the objects to be segmented and allows a locally adaptive correction of the illumination gradient. Determining an appropriate size and shape of the SE is an important task in this application. Figure 3 illustrates the effect of correcting the background non-uniform illumination in a fluorescence image from the above cited example.

Another approach to this problem is presented in [26] in the general context of performing an improvement of the image contrast in grayscale images. Here the background is detected by using a grayscale morphological opening by reconstruction

followed by an erosion operation. This approach avoids the generation of new contours that can arise when working with structuring elements or various sizes. However the method's performance for the particular case of cell images is not addressed in this reference and this could be an open area for research.
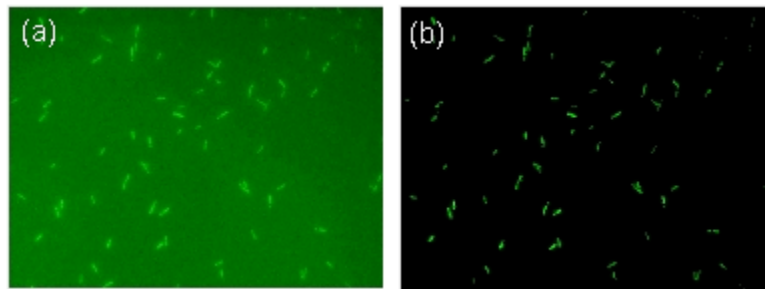

Fig. (3). Correction of non-uniform illumination and background suppression using morphological top-hat with a disk SE of appropriate size. (a) Original fluorescence image of e-coli bacteria (grayscale). (b) corrected image.

2.2. Image denoising

Image denoising techniques in cellular imaging are highly dependent of the noise statistics. There is a wide variety of noise filtering techniques used in DIP: median filters, vector median filters for color images, Wiener filtering, morphological filtering, anisotropic diffusion and wavelet-based filtering among others are significant examples, and this field of research is currently very active. In the case of cell image processing, some techniques have been mostly reported. For example, smoothing by means of a Gaussian filter was used in [27] in the implementation of a single cell based image analysis, for high throughput screening of viral infection.

A median filtering for noise reduction was used in [28] in the context of segmentation of tuberculosis bacilli. In [29] an optimized locally adaptive non-local means denoising filter was employed for cryo-electron microscopy data. In [30] linear and nonlinear spatial filters such as the Gaussian, median, and directional coherence enhancement filter, as well as iterative methods for filtering based on partial differential equations, are implemented and compared.

Morphological filtering was applied in [31] for the purpose of segmentation and labeling of macrophages. In this case filtering served also for the purpose of deleting

artifacts due to the presence of small particles. Morphological filtering can be achieved by a combination of the opening and closing operations.

In [32] morphological operations are used for simultaneous sharpening and noise reduction in high throughput chromosome studies. In [33] a nonparametric regression method is used to denoise fluorescence microscopy images, which makes use of the redundancy inherent to 3D image sequences in order to reduce the effects of Poisson noise. Another example of algorithm for Poisson noise filtering in a low signal to noise ratio environment found in fluorescence confocal microscopy is shown in [34], where noise is removed using spatial and temporal correlations and an anisotropic three-dimensional filter that can be tuned in space and time separately.

The literature review reveals that wavelet denoising has found a widespread use in many applications, ranging from conventional optical to fluorescence microscopy. Having in mind this motivation, we will analyze this approach in some detail in the following sections.

2.2.1. The discrete wavelet transform

The discrete wavelet transform (DWT) is a mathematical tool that can be used very effectively in signal and image analysis. There is a great amount of literature on DWT, and specifically for the DWT-2D (in two variables) used in image processing, see for example [13].

In DWT analysis, a signal $x(t)$ can be described through a linear decomposition as

$$x(t) = \sum_{k} \sum_{j} a_{j,k} \, \psi_{j,k}(t) \, .$$

(2)

In this equation $j, k \in \mathbb{Z}$ are integer indexes, $a_{j,k}$ are the wavelet coefficients of the expansion, and $\psi_{j,k}$ is a set of wavelet functions in t. Notice that the wavelet coefficients $a_{j,k}$ constitute a discrete set, and that the coefficients' values are calculated according to

$$a_{j,k} = \langle x(t) \psi_{j,k}(t) \rangle = \int_{-\infty}^{+\infty} x(t) \psi_{j,k}(t) dt \, .$$

(3)

The DWT obtains the decomposition of the signal $x(t)$ (usually of its sampled version $x[n]$) into a set of orthonormal wavelets and their associated scaling functions $\varphi_{j,k}$ that together constitute a wavelet basis. These functions can belong to different wavelet families that are expressed by the functions $\psi_{j,k}$ which can be generated by dilations and translations of a basic, or "mother" wavelet. These dilations and translations are discrete, and the indexes j and k are respectively related to these processes, that can be expressed for the wavelet functions as

$$\psi_{j,k}(t) = 2^{-\frac{j}{2}} \psi(2^{-j}t - k) \quad j, k \in Z,$$ (4)

In Eq. (4) the functions $\psi_{j,k}$ are dilated in a dyadic form (in powers of two), when varying the values of the index j, and in analogous way translated when varying the index k. In this process, translation is associated with time resolution, and dilation provides scaling, a concept closely related here to frequency resolution. Figure 4 shows examples of wavelets functions that are well described in the literature.
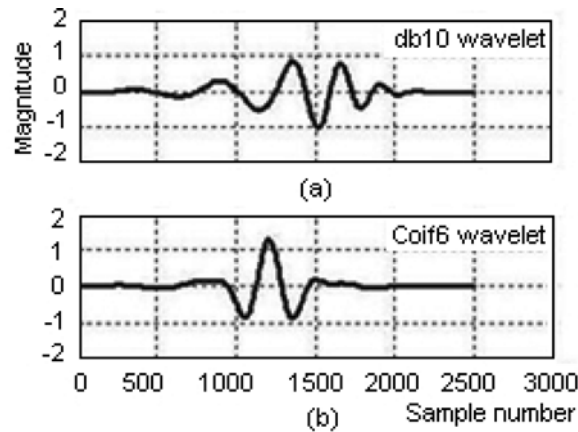

(a)

(b)   Sample number

Fig.(4). Examples of wavelets, (a) Daubechies wavelet db10, (b) Coiflet, coif6 wavelet.

The DWT can be calculated very efficiently through the fast wavelet transform algorithm (FWT), and has many applications in DIP. The result of the DWT is a multi-resolution decomposition, where the signal is successively decomposed in "detail" and "approximation" coefficients. This decomposition is realized through lowpass and highpass filtering for the approximation and for the details respectively, using so called "Quadrature Mirror Filters" (QMF.) There are two types of QMF filters: the lowpass

scaling filter *h*, and the highpass wavelet filter *g*, both with different versions for decomposition and reconstruction.

The DWT is naturally extended to the bi-dimensional (2-D) case of images, where a 2-D scaling function and three 2-D wavelet functions are defined for horizontal, vertical and diagonal details:

$$\varphi(j, k) = \varphi(j)\varphi(k) \tag{5.1}$$

$$\psi^V(j, k) = \psi(j)\varphi(k) \tag{5.2}$$

$$\psi^H(j, k) = \varphi(j)\psi(k) \tag{5.3}$$

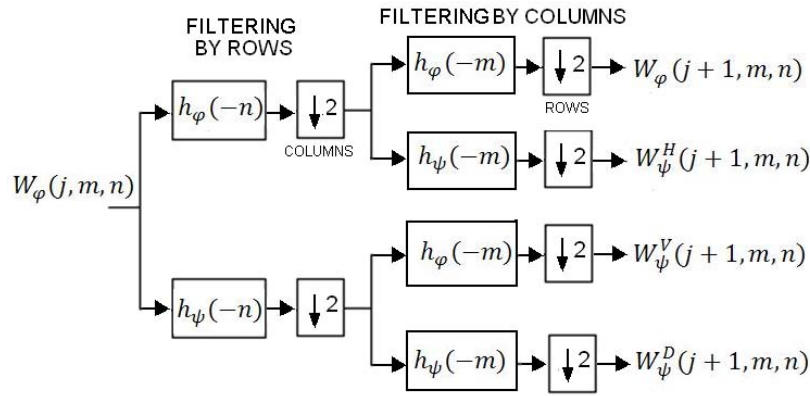$$\psi^D(j, k) = \psi(j)\psi(k) \tag{5.4}$$

Fig. (5). DWT-2D decomposition from level *j* to level *j*+1, notice how the approximation and detail coefficients are obtained by   means of filtering rows and columns in one dimension.

The wavelet decomposition in two variables is separable, which means that the one-dimensional algorithm to calculate the DWT can be applied successively to rows and columns of the image matrix in order to obtain the bi- dimensional DWT, or DWT-2D. This process is accomplished as in the one-dimensional case through lowpass and highpass filtering, as depicted in Figure 5. The typical way to show the images corresponding to the approximation and the different details is depicted in Figure 6. Notice that the inverse discrete wavelet transform can be obtained from the wavelet decomposition structure by means of a filtering and interpolation process. The inverse wavelet transform (IDWT) is an essential part of the wavelet denoising process.

2.2.2. Wavelet denoising

Wavelet denoising is performed through a process which consists in extracting coherent structures from the image using the DWT-2D. In this case, wavelet coefficients that are mostly due to noise, which is uncorrelated with the wavelet basis functions, will have a low absolute value, while coefficients due to the useful image will have a higher correlation's absolute value. Therefore, zeroing the wavelet coefficients with absolute value below a certain threshold provides a very effective noise filtering method. The wavelet transform is very robust to coefficient quantization: suppressing detail coefficients of low absolute values in the original, noiseless image, can have only a relatively small effect on the quality of the image recovered through the inverse DWT.
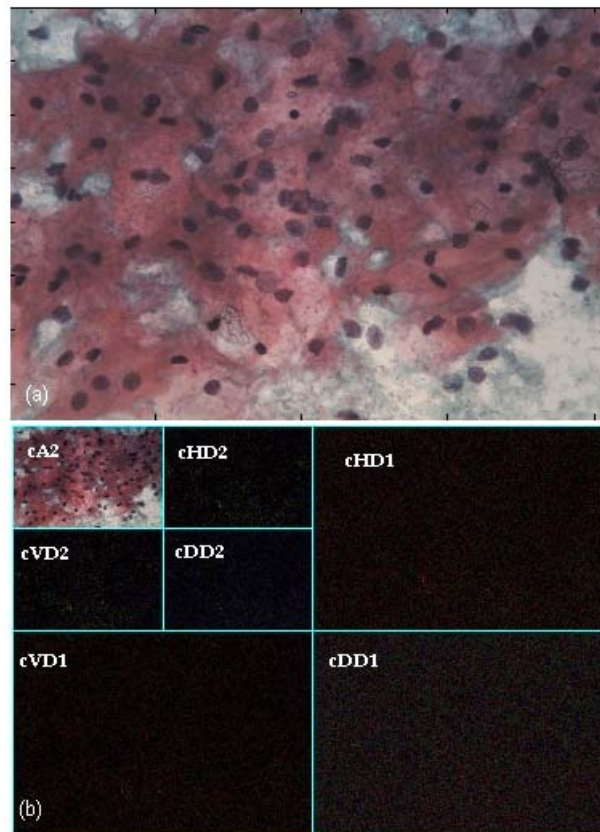

Fig. (6). (a) Cervical cytology image. (b) Wavelet decomposition at two levels. Notice the spatial ordering that is usually employed to organize the approximation and vertical, horizontal and diagonal detail images.

The wavelet denoising algorithm can be summarized as follows:

1. The noisy image is decomposed by means of the DWT-2D for a predetermined level *J*, using some specific wavelet.

2. The absolute values of the resulting DWT-2D detail coefficients are compared to a certain threshold, and the coefficients with absolute value below this threshold are assigned the value zero.

3. The denoised image is obtained through reconstruction by means of the inverse DWT-2D. There are two ways in which thresholding can be performed, named soft- and hard thresholding, which are shown in equations (6.1) and (6.2) and depicted in Figure 7. An example of a noise filtered image is shown in Figure 8.

$$x_{ths} = \begin{cases} x & |x| > t \\ 0 & |x| \le t \end{cases}$$

(6.1)

$$x_{ths} = \begin{cases} sign(x)(|x| - t) & |x| \ge t \\ 0 & |x| < t \end{cases}$$
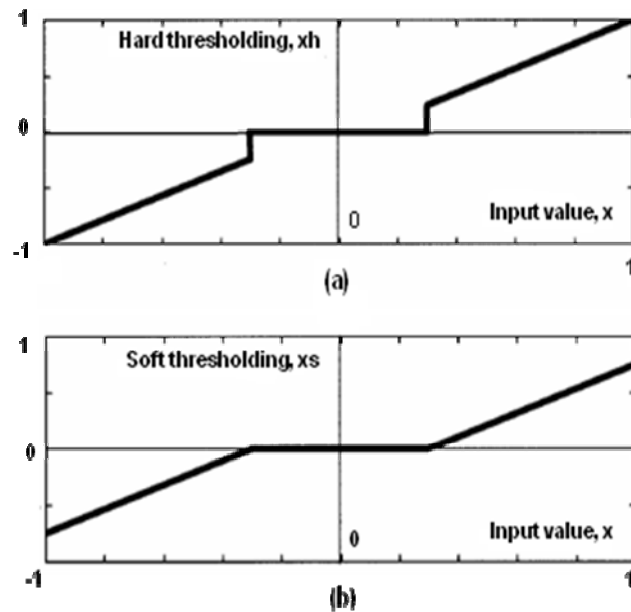
(6.2)

Fig.(7). Input-output characteristics in (a) hard and (b) soft thresholding.

Determining the value of the threshold in wavelet denoising is a relevant issue, because if the threshold value is too conservative (small) the noise filtering effect will be limited, and on the other hand if the threshold value is too large, some valuable information in the image might be lost. Several alternatives to calculate the threshold value from the image parameters have been developed, and a careful selection is to be

made in order to achieve a successful denoising. A graphical example of wavelet image denoising results is shown in Figure 8.

Consider now the case of fluorescence microscopy, where noise has a Poisson probability distribution due to the physical nature of the process. This means that there is dependence between the noise variance and mean value, and in this case a variance stabilization transform is firstly applied to the image data to remove this dependence, usually the so-called Anscombe transform or some related procedure. Then some alternative of wavelet denoising is applied. In what follows we will show several examples of these techniques. In [35] the general problem of Poisson noise removal is addressed. Here a variance stabilizing transform is used to obtain a Gaussian process form the original Poisson one, and then denoising is performed using wavelet filter banks, as well as ridgelets and curvelets (transforms in which the basic elements are directional and anisotropic, making them more suitable for some image processing tasks). Then the significant coefficients are detected using classical hypothesis testing. This work is of potential use in the area of cell image processing. Confocal microscopy is used in [36] for the study of events related to intracellular calcium concentration. Wavelet denoising was used successfully in this case, where threshold selection was derived from the standard deviation of the noise contaminating the signal. A fast algorithm is presented in [37] to reduce the Poisson noise in fluorescence microscopy, based in the use of the Haar wavelet and a technique of linear expansion of thresholds. This solution showed to have a performance comparable to other multiscale methods but orders of magnitude faster. A high content screening application for automated monitoring of cell populations is described in [38], in which denoising is accomplished through wavelet frames (where decimation at decomposition levels is omitted), this approach proved to be robust to local noise variations and allows segmentation even with low contrast to noise ratio.
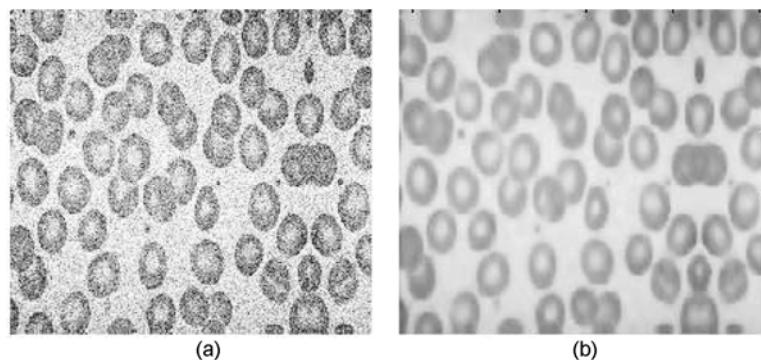

(a)   (b)

Fig. (8). Image denoising, (a) image contaminated with Gaussian noise and (b) image after wavelet denoising.

2.3. Image deblurring

Blurring is an impairment that occurs in microscope imaging, which is usually mitigated through deconvolution techniques. This effect is particularly important in 3D fluorescence microscopy, where the distortion introduced by the microscope reduces the resolution attainable by the system, imposing limitations to the analysis of the specimens under study. An overview of the deconvolution methods used in 3-D fluorescence microscopy is presented in [39].

There are two sources of blurring in fluorescence microscopy: convolution of the object with the microscope point spread function (PSF), and random noise. The PSF is equivalent to the impulse response of the optical system, assuming linearity. There are optical methods to reduce blurring by rejecting the defocused light before it is detected, which need some computational processing to improve the effects of anisotropy, as well as purely computational methods. The general scheme of the blurring process and deblurring by image deconvolution is depicted in Figure 9.
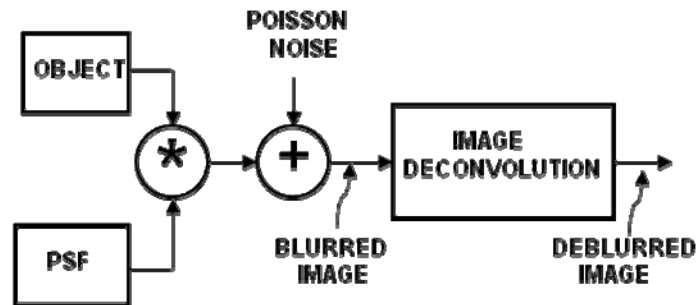

Fig. (9). General scheme of the process associated to image deconvolution, where convolution is denoted by the asterisk symbol.

In fluorescence microscopy, a three-dimensional (3-D) image of an object is acquired from a set of 2-D images, obtained by focusing the microscope at different

planes. There are various sources of distortion in an image acquired in this way: flickering of the lamp, non-uniform illumination, defocused light, attenuation, geometrical effects and Poisson noise related to the photon emission during fluorescence. In computational deconvolution for 3-D images, the algorithm processes a stack of 2-D slices to reduce their out of focus contribution to the image.

Given that the PSF is the 3-D impulse response of the microscope system, assuming a linear model and Gaussian additive noise, the resulting image will be given by

$$f(x,y,z) = h(x,y,z) * o(x,y,z) + n(x,y,z) \qquad (7)$$

where $f(x,y,z)$ denotes the blurred microscopy image, $o(x,y,k)$ is the original object, $h(x,y,z)$ the PSF, * the convolution operation, and $n(x,y,z)$ is the noise process. In real cases, the background Poisson noise and the setup parameters used when measuring the PSF should be taken into account. Another issue is that Poisson noise constitutes a better model than Gaussian noise in low light conditions, where the signal to noise ratio is poorer.

There are various methods for image deconvolution, and among them inverse filtering will be briefly described due to its straightforward interpretation. When the PSF $h(x,y,k)$ is known and a noiseless image is assumed, the convolution property of the Fourier Transform when applied to equation (7) leads to the so-called inverse filtering, given by

$$\hat{o}(x,y,z) = F^{-1} \left\{ \frac{F(v_x, v_y, v_z)}{H(v_x, v_y, v_z)} \right\}, \qquad (8)$$

where $\hat{o}(x,y,z)$ is the deblurred image, F^{-1} is the inverse Fourier transform operator, F and H are the Fourier transforms of the blurred image and the PSF respectively, and v_x, v_y, v_z the spatial frequency variables in the Fourier transform. Taking into account that $H(v_x, v_y, v_z)$ is bandlimited and in order to make possible the calculation of equation (8) when the values of $|H|$ are very small, the truncated inverse filtering is defined as

$$\hat{o}(x,y,z) = \begin{cases} F^{-1} \left\{ \frac{F(v_x, v_y, v_z)}{H(v_x, v_y, v_z)} \right\} & \text{if } |H(v_x, v_y, v_z)| \geq \varepsilon \\ 0 & \text{if } |H(v_x, v_y, v_z)| < \varepsilon \end{cases}. \qquad (9)$$

Inverse filtering requires performing a previous evaluation of the PSF, which can be realized experimentally by obtaining the images of point-like objects directly in the microscope and acquiring them. This method has the limitation that point objects lead to very poor signal to noise ratio. PSF can be evaluated also analytically, using the equations of diffraction theory, or computationally using blind deconvolution algorithms, which allow a simultaneous evaluation of the PSF and the object's image.

There have been recognized six classes of computational algorithms for 3-D image deconvolution: neighboring and no-neighboring, linear and nonlinear methods, statistical methods and blind deconvolution. Some application examples in cellular imaging are examined in the following. In [40] a realistic Poisson-Gaussian noise model is used in a formulation devoted to obtain an optimal regularization parameter and the resulting deconvolution algorithm was used in a real 3-D wide-field microscopy images with good results. In [41] the authors developed an algorithm that performs deconvolution when a thick specimen is imaged in a brightfield microscope, which prevents focusing the entire object. The problem of deconvolution and chromatic aberration corrections in multi-dimensional confocal microscopy is addressed in [42] in order to achieve an accurate determination of colocalization between biological macromolecules at the subcellular level. The developed method implies the measurement and use of the system's PSF. An algorithm for wavelet regularized deconvolution for 3-D fluorescence microscopy was developed in [43], which accelerates the deconvolution process for real data applications. Blind deconvolution is used in [44] for the specific application of image restoration in 3-D microscopy. Here a new PSF regularization method through learning-based algorithms is introduced for applications in wide-field fluorescence microscopy. The algorithm developed allows reconstruction results with high resolution and low noise levels for real world images.

3. IMAGE SEGMENTATION

Segmentation is the process by means of which an image is subdivided in its constituent parts or objects, according to some criteria. This is one of the fundamental processes in any image processing or computer vision system, because it allows

extracting from the image the objects of interest in order to perform further analysis tasks such as description, pattern recognition or classification. The segmentation process ends when the relevant objects for the specific applications have been isolated. At this stage, the image will be constituted by connected sets of pixels that belong to the regions of interest and to the background, and that share some adjacency property. From a mathematical point of view, a segmentation of an image *I* defined in the domain D_I, is a partition of this domain into *N* disjoint segments, which are nonempty sets X_n whose union is the domain D_I,

$$D_I = \bigcup_{n=1}^{N} \{X_n\}$$
.   (10)

Segmentation is a topic widely studied in the general literature on DIP, see for example [13]. In the particular case of cell image processing, segmentation may pursue a wide variety of purposes and face numerous technical challenges. A concise and updated survey of the usage of the diverse segmentation methods in cell imaging can be found in [45]. The complexity of segmentation in cellular imaging is due to the multiple morphologies that can be found, the various modalities of microscopy currently used and the diverse possible purposes of the study to be made. These studies can include the analysis of the cell internal structures, which in such cases become the objects to be segmented. A common partial result of a segmentation process in cell imaging is a binary image, composed of the segmented objects and the background. These binary images are then used to select the regions of interest for their study.

The purpose of this section is to review the segmentation techniques that are mostly used currently, to provide an approximation to the state of the art in cell image segmentation, and to discuss a set of representative examples. There are a vast number of segmentation techniques which have been developed for general applications in digital image processing, and in regard of cell images, there is not a method so far whose performance can be considered as the best in all situations, and such a solution is not foreseen currently. This means that there are a great number of ad hoc solutions for segmentation of specific types of images. Among the multiple segmentation algorithms that have been reported in the literature, the morphological

20

watershed transform and the active contours with level set techniques, both with many variants, are probably the most widely used currently in cell image processing. These methods will be reviewed in some detail in sections 3.1 and 3.2.Several other methods can also be found, of which a brief overview is also to be given in section 3.3. An important problem that usually appears in cell image segmentation is the necessity of separating cells that are touching or overlapping, and this topic will be addressed in section 3.4. Finally, it is important to recognize that given the large variety of segmentation techniques available, evaluating the effectiveness of a particular segmentation algorithm for a given application, as well as establishing metrics that allow comparisons between methods is of paramount importance. Having this motivation in mind, a brief summary and some discussion on segmentation eva-luation methods is presented in section 2.5.

3.1. Image segmentation using the watershed transform

The watershed transform as a segmentation tool is based in the concept that the intensity of an image can be represented as a surface in a 3-D space, in which the gray level is considered as an altitude. This image structure shares the properties of topographical surfaces, and as such it can exhibit slopes, hills, valleys and plateaus. This concept is used in mathematical morphology to define many grayscale morphological processing operations that can be applied to an image.

The watershed transformation is a morphological process that can be used with high effectiveness for image segmentation, for which a thorough study can be found in [24]. Of primary importance for this algorithm are the following concepts, applied to the intensity surface of an image:

- Regional minima: connected sets of points for which there are not surrounding pixels having a lower level.
- Watershed catchment basins: sets of points such that a drop of water put on any of them would flow towards a well defined minimum.
- Watershed ridges or lines: sets of points such that a drop of water put on one of them would flow indistinctly to more than one minimum.

The watershed transformation can be interpreted on the basis of the so-called immersion algorithm, in the following way:

1. A small hole is punched in the bottom of each local minima of the image's intensity topographical surface.
2. The whole image surface is gradually immersed in a recipient full of water, and the water will begin to flood the local minima and their associated catchment basins. The surface of the water in each catchment basin will grow as the water level increases.
3. As the water level increases in a given catchment basin, it tends to reach the surrounding ridge at some point, which would cause the water to overflow to an adjacent catchment basin. At this moment, a dam is constructed by means of a morphological algorithm, in order to prevent this overflow. This process is repeated for all the catchment basins in the image.
4. At the end of the process all the catchment basins will be isolated from one another in such a way that a segmentation partition is established.
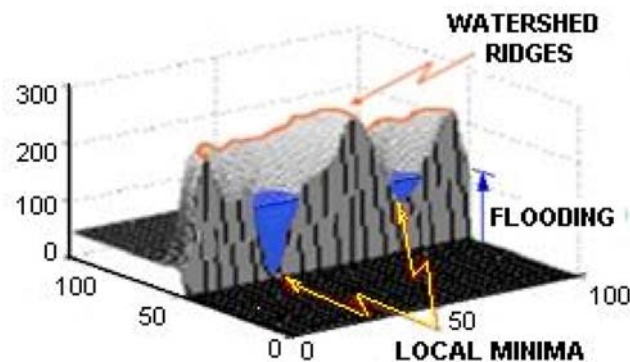

Fig. (10). Illustration of the watershed immersion algorithm for image segmentation.

The immersion process will eventually finish when only the tops of the dams are visible above the water surface, these are precisely the watershed lines. The watershed immersion algorithm can be considered as a combination of region growing and edge detection process, which assigns pixels to the most similar neighboring region starting from local minima. This algorithm can be completely implemented using morphological image processing operators. Figure 10 depicts a three-dimensional graphical illustration of the watershed immersion algorithm as it can be interpreted in an intuitive way.

In order to improve the watershed transform segmentation, some pre-processing techniques are to be used on the grayscale image. For example, applying the watershed transformation to the image's gradient instead of the original image, tends to reinforce the watershed ridges of the image's intensity surface and leads to a better watershed segmentation. This is illustrated in Figure 11(b), in which the morphological gradient of the image 11(a) was calculated.

The watershed transform tends to produce an over-segmentation, which in some cases can be severe. This is due to the presence of local minima inherent to the image or to noise contamination, and suggests the convenience of noise filtering prior to segmentation. The mentioned effect is worst when the image of the gradient is employed, because the derivatives tend to reinforce the noise level in the image.

One method often employed in order to reduce over-segmentation is the use of markers. Markers are connected components located in the image, which are used to limit the number of segmentation regions in the gradient (or any other) image. Markers can be internal when placed inside the objects of interest and external when they belong to the background. There are various DIP techniques to create internal and external markers. We mention minima imposition as another morphological technique used together with markers [24]. Figure 11(c) and (d) illustrates the usefulness of markers in watershed segmentation.
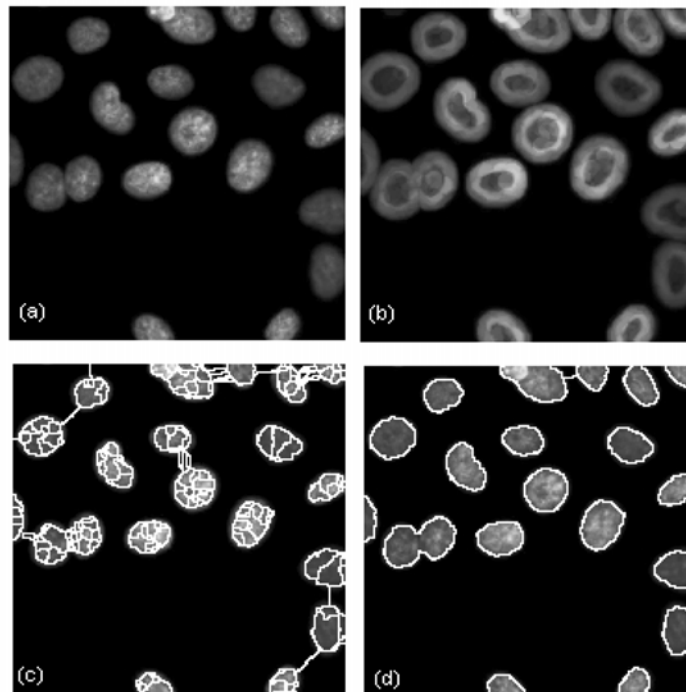
Fig. (11). (a) Original image to be segmented, (b) morphological gradient of the image in (a), where the enhancement of the borders can be appreciated; (c) watershed segmentation without markers, notice the severe oversegmentation, and (d) watershed segmentation using markers and minima imposition.

Now we present some illustrative examples of the use of the watershed transform in specific experiments. In [46] the watershed segmentation is used in the context of high content screening applications in a toxicity assay. The full methodology uses also connected filters and granulometries for segmenting cells of different size, contrast and other attributes. In this work, specific markers are used to facilitate segmentation of the cells' contours, other markers to highlight the nuclei and marking with green fluorescence protein (GFP) to quantify the effects of the toxics. The watershed transform was used with inner and outer markers, and over a gradient function associated to the contour of the cytoplasm. After segmentation, other global parameters associated to the cell populations in the images are calculated, especially the evolution of the spatial aggregations of cells using morphological granulometries. In [30] a unified framework is developed to segment surface stained living cells from 3-D data sets of fluorescent images. Here the previously fluorescence-labeled cells are subject to a pre-processing consisting in background suppression and ridge enhancement by means of filtering. Then marker-controlled watershed segmentation was performed, as well as segmentation by active contours (to be discussed later in this article) and a thorough evaluation of the results was made by comparison to a ground truth using similarity measures, obtaining slightly better results for the wastershed method.

Simultaneous segmentation and classification of heterogeneous populations of cell nuclei in batches of 3-D confocal stacks of microscope images was addressed in [47], making use of watershed segmentation. The goal here was allowing segmentation in tissues containing multiple cell types with different nuclear features. The gradient-weighted watershed algorithm produces here an over-segmentation and a method for fragment merging was developed, using multiple objects models and linear discriminant analysis to classify the candidates for merging. The authors obtained classification and

segmentation accuracies above 93% for images of different regions from a rat's brain. Segmentation of *in vivo* Arabidopsis Thaliana cells in a time-lapse confocal microscopy study was made in [48] using the watershed transform. Here a technique to reduce over-segmentation was also developed, based on edge strength along the line that connects adjacent centroids in the cells. This allows elimination of bad and over-segmented cells by means of an evaluation using support vector machine (SVM) classification. In [49] a combination of interactive manual and watershed segmentation is employed to efficiently track morphological changes of cells in living tissues, in time lapse movies obtained from a laser-scanning confocal microscope. Here manual interaction is used to create and manipulate seeds, or markers, in order to facilitate further watershed segmentation. The algorithm neither require previous definition of parameters nor trained human experts, and showed good segmentation results in reasonable computation time when compared to other similar existing tools.

Watershed segmentation is frequently used to separate the components in cell aggregates, and this specific topic will be discussed later.

3.2. Active contours and level sets in image segmentation

Active contours constitute a widely used approach for image segmentation and are used also for applications like motion tracking. This methodology is based in the use of deformable contours that can dynamically adapt to the shapes or motions of different objects. There are two basic formulations in segmentation with contours: the so-called snakes and the level sets approach. The evolution of the contours can be based in edges or in regions. For example, in edge-based active contours, an edge detector, like the image gradient, is used to find the boundaries of the region to be segmented, and the contours are attracted to these boundaries. In the case of region-based active contours, it is the statistical information on the image intensity inside the regions to be segmented which is used to drive the process of contour evolution.

In the case of cell segmentation, the level sets approach is preferred because snakes cannot adapt simultaneously to the boundaries of more than one object: the contours in this case cannot change their topology during the evolution process. In the case of cell images, in which usually there are simultaneously various objects (cell, nuclei) to

segment, snakes are not capable of splitting in multiple boundaries. This is not the case of level sets, for which the contours can adapt to multiple boundaries or even merge whenever it is necessary. For this reason, the level sets approach is the one to be considered in this section.

Level sets were introduced in [50] and have had further development since that time. In this formulation, the contours are represented implicitly by means of a bi-variate level set function, $\phi(x,y): \Omega \to \Re$, defined in the domain Ω of the image $I(x,y)$. One particular level of this function (commonly the zero level) is defined as the contour, such as

$$C \equiv \{(x,y): \phi(x,y) = 0\}, \forall (x,y) \in \Omega \tag{11}$$

The evolution of a level set function, together with the contour defined as the zero level, is exemplified in Figure 12. Notice that as the level set function $\phi(x,y)$ -which has the form of two inverted cones- decreases from an initial condition (the cone vertices move downwards), the contours C corresponding to the level set propagate outwards in the zero level plane. The evolution of the contour C is in correspondence with the evolution of $\phi(x,y)$.

If the contours are defined as the border between a positive and a negative area, they can be associated to the sign of $\phi(x,y)$, and the initial level set function $\phi_0(x,y)$ can be a signed distance from the initial contour,

$$\phi_t 0 \, (x,y) = \{\phi(x,y): t = 0\} = \pm D((x,y), P_\perp(x,y) \, (C_t 0 \,), \qquad \forall (x,y) \in \Omega \tag{12}$$

where D is a distance function between some point (x, y), and $P_{x,y}(C_0)$ is the nearest pixel on the initial contour $C_0 = C(t = 0)$.

The deformation of the contours in the level set method is represented usually by means of a partial differential equation (PDE) that evolves according to the magnitude of the gradient, as

$$\frac{\partial \phi(x,y)}{\partial t} = |\nabla \phi(x,y)| \left(\sigma + \partial K(\phi(x,y))\right).\tag{13}$$

In equation (14), σ is a constant speed term that determines the movement of the contour and the function $K(\cdot): \Omega \to \Re$ is the mean curvature of $\phi(x,y)$ given by

$$K(\phi(x,y)) = div\left(\frac{\nabla\phi}{\|\nabla\phi\|}\right),$$

where equation (13) can be interpreted as a description of motion motivated by a PDE.

The process of image segmentation by means of level sets begins with a user-defined boundary (a contour or set of points) and then the contour evolves in accordance to the above mentioned PDE. A stopping function is defined as a positive and decreasing function of the image gradient, such that the contours move in a normal direction at some speed and stops evolving once the stopping function is close to zero, when the contour delineates the borders of the objects. A property of the level sets segmentation method is that the contours can split or merge according to changes of topology in $\phi(x,y)$. This means that more than one boundary can be detected at the same time, and also that several initial contours can be established. This property makes the method particularly appropriate for cell or nuclei segmentation.
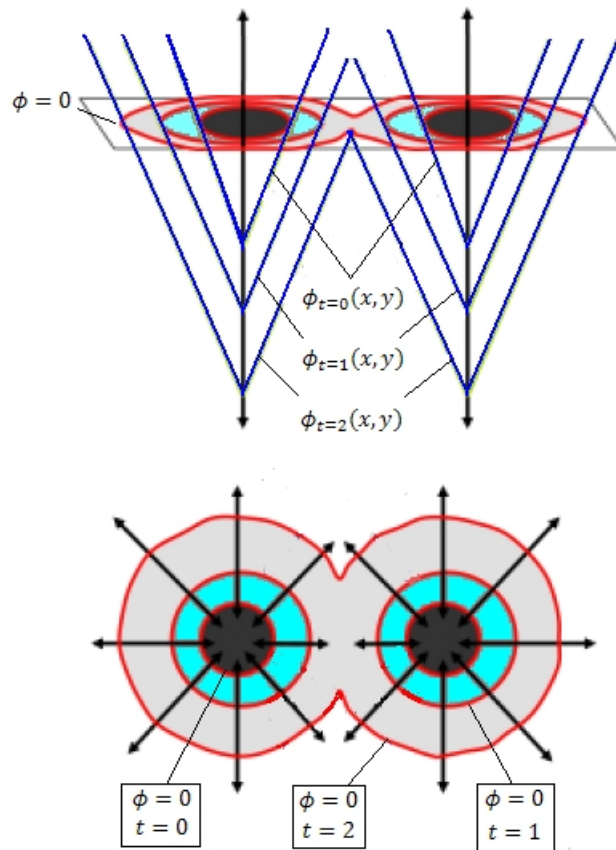

27

Fig. (12). Contour evolution in the level set formulation, (a) evolution of the level set function $\phi(x,y)$, and (b) the corresponding evolution of the contour C. Notice that in this case two contours initially separated merge as a result of the contour evolution.

A first example of the application of level sets in cellular image processing can be found in [51], where it is performed the interpretation and measurement of the architectural organization of mitochondria in electron microscopy images. The images of mitochondria were firstly pre-processed by denoising and closing interrupted structures using an approach based in edge and coherence enhancing diffusion. This allows noise removal and structure closure at certain scales, while preserving both the orientation and magnitude of discontinuities. A variational level sets method was then used for contour extraction. In [52] the level sets method was applied to multi-cell segmentation and tracking in time-lapse fluorescence microscopy and contributed an algorithm which improves the robustness against noise as well as the segmentation and tracking accuracy while reducing the computational cost in comparison to previous similar algorithms. The algorithm's performance was evaluated for real fluorescence microscopy images from different biological studies. In this work, watershed segmentation was also used as a complementary algorithm to separate touching cells. In [53] the problem of segmenting stem cells was addressed through multilevel-sets segmentation. Given that the stem cells have complicated morphologies composed by blobs (the cellular body) and curvilinear structures, the authors introduced the use of multi-scale curvilinear structure detectors for these structural components, and used the detected structures as initial cell contours for multi-level sets. Results were validated for embryonic and neural stem cells, with more than 90% of cell blobs detected correctly.

In [54] level sets were used in automated eukaryotic live cell analysis of the four phases of the cell cycle during replication, in a high-throughput and high-content environment. The tracking problem was addressed here as a spatio-temporal volume segmentation problem, and the segmentation of the G2 and S cell phases is made using level sets. The developed method allows the automatic analysis of the cell phases during extended periods of time without the need of staining the nucleus. A software package to analyze relevant characteristics of neurites, like length and complexity, was developed in [55]. In this case, both level sets and watershed methods were

28

employed. Here the nuclei were firstly detected using a level sets method with a specific initialization, and then the entire cells were segmented using also level sets but with a different initialization. In this case, one level set function is used to segment all the cells in order to have a better computational efficiency. Then in order to prevent merging of different regions during the evolution of the level set function, the topological dependence between regions is controlled using a dynamic watershed algorithm. All these were integrated in a software system called *NeuronCyto* that allows analyzing the neurites quantitatively.

In [56] an active mask algorithm is proposed, that combines the advantages of active contours, multiresolution, multiscale and region growing. This method was applied to fluorescence microscopy images imposing topology preservation. Here an increase in computational speed was achieved by segmenting a coarse component first, and then making a refined segmentation at finer levels. The algorithm was compared to seeded watershed and showed a better performance in segmenting fluorescence microscopy images.

Level sets have demonstrated to possess high ability to segment objects with varying intensity and shape, to deal effectively with topological changes, and to deal with both 2-D and 3-D image sequences, however some limitations are to be taken into account at the moment of selecting this method for its use in an application: the algorithm performance is very sensitive to the parameters, requiring tuning for each new dataset, there are difficulties to select a good stopping criterion for the curve evolution, the speed of convergence is influenced by initialization and the method tends to be time consuming. Research on level sets applications to cell segmentation is very active currently.

3.3. Other methods used in cell segmentation

There are numerous works in which other methods, as well as combinations of those described above, have been developed. A first example can be found in [57] in which the relative simplicity of cell images allowed segmentation by using upper and lower gray intensity thresholds. In [58] a sliding band filter was introduced as a pre-processing step for joint segmentation of nuclei and cytoplasm. This filtering allows detecting the

convex shapes in order to determine the cells' nuclei and cytoplasm locations and shapes. In [59], a machine learning method was used for segmenting cell images from blood and bone marrow. Here three mean-shift procedures [60] are used to find the local clustering modes (maximum of the probability density function in the RGB color space) associated to the nuclei, mature erythrocytes and background regions. Then a support vector machine (SVM) is trained using uniform sampling from the three modes to find more nuclei pixels. The nuclei regions are conditionally dilated in the high gradient pixels to obtain parts of the cytoplasm pixels, and a second SVM is trained with a set of samples from the cytoplasm and the three modes previously determined. Two classification modes are obtained using learning and sampling on-line. Finally a last SVM is used to segment the image extracting the whole leukocytes. The method is compared to specific watershed-based and thresholding-based algorithms and showed better values in a confusion matrix which contains the information about the classification of pixels. Another example of the use of SVM in segmentation appears in [61] for white blood cell segmentation in multispectral images, where segmentation is performed at the pixel level. The mean-shift algorithm was used also in [62], in a system oriented to measuring the proliferation rate of cancer cells.

In [63] it is addressed the problem of separating nuclei from background in cell images from a p53 immunohistochemistry experiment, as a problem of color cell image, two-class segmentation (separating cells from the background). The authors developed a supervised, learning-based two-step procedure where thresholding is used after converting the images from color space to grayscale. A marker detection method for use in watershed segmentation is also presented, to be used in the separation of overlapping nuclei.

In [64] two segmentation methods based in the use of color information were applied to immunohistochemical high-resolution images of tissue samples stained with marked antibodies. In this application, different stains with inhomogeneous distribution were used, and different tissue components were considered, showing morphological variations and heterogeneity of the regions to be recognized. The first segmentation method uses unsupervised color clustering and is capable of recognizing the cancerous areas in the specimen under analysis. The second method uses color separation and

morphological processing in order to segment the nuclear membranes of the cancerous cells. Nuclei were separated from the background by means of local analysis of the intensity distribution in the neighborhood of each cell, and clusters were separated using a watershed algorithm. The results were compared to segmentation through support vector machines (SVMs) and active contours and showed a better performance, comparable to that obtained with manual segmentation. Color information was used in [65] for the segmentation of images of fibrosis in the liver. The algorithm works in two steps: (a) segmenting Sirius red–stained hepatic fibrosis from cell pixels in the image by thresholding the green component, based on enhanced joint clusters of green–blue vectors, and (b) separation of irregular fibrosis areas from the hepatocyte nuclei of relatively uniform size and shape, using morphological operations. Results showed that fibrosis regions were identified with high accuracy. Segmentation of tuberculosis bacilli is presented in [28], using a moving K-means clustering employing the green component in the RGB color space and the R_y component of the C-Y color space, in order to segment the TB bacilli from the background.

In [66] the use of wavelet transform decomposition was introduced to complement the traditional watershed transform segmentation. The problem addressed was the accurate segmentation of cell nuclei for studies about 2-D spatial distributions in terms of relative and radial distances of fluorescence in situ hybridization (FISH)-labeled DNA sequences in inter-phase nuclei. A modified multiscale (wavelet based) technique was used for enhancing the image intensity at the boundaries of clustered nuclei (CN). Then multiscale thresholding, based on entropy information from multiple scales, was applied for handling non-uniform background intensity variations, and statistical pattern recognition tools were used to obtain the input parameters required for segmenting cell nuclei, combining watersheds and region merging. A comparison of the output from automatic classification to manual segmentation was then made, showing good results. In [67] a segmentation method is developed to obtain the regions of interest (ROI's) in cell images, oriented to content-based retrieval in diagnosis systems based on cytology and histophysiology. The system obtains an adaptive attention window (AAW) whose purpose is to determine the rough position of relevant ROI's. The AAW is obtained through a process that uses a luminance map and quad-tree split based on human

perception during a pre-processing stage. After this, region-level segmentation is performed within the AAW and the final ROIs segmented using background removal and region clustering. Similar adjacent regions are merged sequentially if they satisfy some conditions. The system was tested by comparison to the mean-shift segmentation algorithm and to manual segmentation, showing results closer to the latter, in terms of the fraction of actual ROI's and abnormal ROI's that were identified.

An approach for high content screening applications is presented in [68]. Here segmentation is performed after noise removal and it is based in thresholding of the histogram using a three-class (background, cytoplasm and nucleus) *K*-means algorithm. In this process, the pixels are assigned as elements of the cell surface (nucleus + cytoplasm, defining mask *M*) or to the background. An algorithm to find the cell centers as local intensity maxima is applied, which also locates the boundaries between adjacent cells as ridges of minimum intensity inside the cell surface. Then a region growing algorithm plus some refinements were applied. The seeds were the previously defined cell centers and the outer limit was *M*. The method was tested for four different types of cells, and though it is fast and relatively simple, it starts from a set of assumptions that could mean limitations to its use: cells should be uniform in size, convex and symmetric in shape, stained with a single color band, and the nucleus should be as bright as the cytoplasm. An application of thresholding segmentation in time-lapse fluorescence microscopy is reported in [69]. In this case, a first segmentation step was performed by means of adaptive thresholds, after a preprocessing for image enhancement. Then morphological processing was used to eliminate small noise artifacts and "holes" in the nuclei. This first segmentation was complemented with the use of distance transform and watersheds to separate touching nuclei, a topic to be discussed later in this article. The process leads to some oversegmented nuclei that are merged by means of a hybrid merging algorithm after the watershed segmentation.

In [70] a combined method for segmentation of leukocytes and erythrocytes in blood smear images is presented. Here pixel-wise classification combined with template matching is used to locate erythrocytes and later a level-set method is used to obtain the exact cell contours of leukocyte nucleus and plasma regions as well as erythrocyte regions. Some specific problems in segmentation of living cells are addressed in [71] for

phase contrast images of bone marrow stromal cells. In this case, it was not possible the use of fluorescent markers or histological stains to facilitate the segmentation process, and a bright halo appears around cell borders, making difficult the detection of edges. A rough segmentation was performed using a standard deviation mask with thresholding, which was refined later by means of a mean and median filtering process. Results were used for pattern recognition in these images with good results. The main limitation of the system was that it does not segment touching cells and tend to fail for images with insufficient background area.

Segmentation in confocal laser scanning microscopy images is addressed in [72]. In this case the approach was a statistical segmentation method. The model used for the images was a linear mixture of background and fluorescence signals, which unifies the description of high- and low- intensity classes and background without the need of model selection mechanisms. Then model fitting is made using an expectation-maximization approach. Satisfactory results were obtained in tests made with Yeast and HeLa cells.

Segmentation of living cells, particularly neutrophils and lymphocytes, was addressed using a combination of texture- and contour- based techniques in [73]. A first coarse texture-based segmentation is made using the mean and standard deviation of the grey level for texture blocks, from which a binary image is obtained through thresholding. An image contour is determined using a gradient operator, after some morphological operations. The method described is not fully automated, which constitutes a limitation. Dynamic programming for cell segmentation was used in [74]. A semi-automatic algorithm is presented here for segmenting fluorescence-labeled cells or nuclei from 3-D tissue images. Segmentation starts with semi-automatic delineation of 2-D objects in a user-selected plane, using dynamic programming (DP). This allows locating the border with an accumulated intensity per unit length greater than any other possible border around the same object. Then the two surfaces of the object in planes above and below the selected plane are found using an algorithm that combines DP and combinatorial searching. Segmentation errors are corrected in an interactive way. An assessment was made both quantitatively with simulated data and visually, showing good results.

In [75], segmentation through an algorithm called stable count thresholding (SCT) is shown. It is intended to segment nuclear compartments in image stacks of confocal laser scanning microscopy, with the purpose of performing objective and quantitative analysis of the three-dimensional organization of these objects through statistical methods. The SCT algorithm applies thresholding to the three color components in the voxels of the image stacks, and then uses a criterion to determine when the voxel count is stable for a given threshold. The algorithm was tested using stacks of simulated images and fluorescent beads and showed results close to manual segmentation, although comparison to other segmentation alternatives is not shown.

A segmentation method is introduced in [76] to study the three-dimensional redistribution of nuclear components in human mesenchymal stem cells. Here to segment the details of interest in the probe image, a derivative scale-space method oriented to variable and noisy background was used. The image is convolved with Gaussian kernels of different widths to produce a Gaussian scale space of the image. Then after some manipulation, segmentation by thresholding is applied. Afterwards, another algorithm using an iterative threshold selection method is used to segment the nuclei. The proposed method in general has the limitation of requiring some human intervention in order to separate touching objects.

A system for the automatic analysis of the Papanicolaou Smears test is presented in [77], which is used for screening precursor lesions of cervical cancer. In this case the cell nuclei are recognized as the more informative regions, and this determined as the main target to achieve an exact segmentation of nuclei. The segmentation method developed specially for this application is based in the evaluation of the pixel colors in the HSI color space. Membership functions were determined, based in criteria from human experts, and using the pixels' hue and saturation, in order to classify them as belonging to the inner or the edge regions of the nuclei. Three color classes were considered for this: pink, blue, and transparent. Then the degree of membership or the pixels to the nucleus inner and edge regions was determined. The algorithm was evaluated in terms of the effectiveness in detecting the different classes of nuclei, showing good results. Another example related to image analysis in the Papanicolaou

test is presented in [78], where the goal is separating the nuclei from cytoplasm in the cell regions. These images are characterized by inconsistent staining, poor contrast, and the presence of overlapping cells. The authors developed a segmentation method which involves automatic thresholding to separate the cell regions from the background and the use of multiscale watershed transform in order to construct a hierarchical segmentation tree, which allows identifying the nuclei at different scales and separate them from cytoplasm within the segmented cell regions by means of a binary classifier. Evaluation of the method was made by comparing the segmentation results to a manually constructed ground truth in a database of real images, with good results.

A method for segmentation of the cell membranes in computerized immuno-histochemistry is presented in [79]. In this application conventional methods like watersheds or level sets cannot be used due to lack of intensity information, and a method called "detection of final cellular membranes" is introduced. This method uses the (detectable) cell nuclei positions to delineate approximate membranes and the color information to make a refinement in the membranes' positions, calculated as the barycenters of brown pixels along a previously defined scan line. Results are evaluated by comparing to a manually obtained ground truth, showing better results in comparison with active contours. A coarse-fine segmentation method is presented in [80], in which information from both brightfield and fluorescence image is used. The coarse segmentation is performed either using texture information from the brightfield image or intensity thresholding in the fluorescent image. It is intended mainly to produce markers for the fine segmentation, which is made through the watershed transform of the gradient image. Results are evaluated using neural stem cells and synthetic images, both visually and numerically and no comparison to other segmentation alternatives is provided. The method has as limitation the need of some interactive user-defined parameters. Reference [81] introduces another segmentation method for cell nuclei segmentation based in graph-cuts binarization, constrained multiscale Laplacian of Gaussian filtering and further refinement based in a graph cuts algorithm. Results were evaluated using in vitro and in vivo images of cancer histopathology studies and measuring errors like nuclei touching or overlapping in some degree, errors in

binarization as well as sensitivity (recall) and positive predictivity (precision), with good results although no comparison to other methods is provided.

Some other examples that include segmentation techniques will be presented briefly in the section on current applications.

3.4. Segmenting touching and overlapping cells

Segmentation of touching or overlapping objects, as can occur for some classes of particles in a more general context, is a challenging problem for automated image analysis in various fields. It is a common situation that cells that touch or overlap, forming aggregates, appear in microscopy images. Separating the cells clumped in aggregates through segmentation is critical in applications like cell identification and classification. Segmentation of overlapping cells is usually a subsequent step, after the initial segmentation of the image by means of some method that is not capable of detecting or decomposing these aggregates. Once the aggregates are found, the task is to separate them into their constituent elements. This is performed by means of a second segmentation process, in such a way that the features of these elements can be analyzed individually.

A well-known method for segmentation of aggregates in cell images, is based in the calculation of the distance transform map of the image obtained as a binary mask, in the above mentioned initial segmentation process. After this, the watershed transform is applied to the distance map, usually introducing adequate markers. The distance transform of a binary image is defined as follows [13], [24]: for every pixel x in set A, $DT_A(x)$ is the distance from x to the complement of A,

$$DT_A(x) = \min\{d(x,y) \qquad y \in A^c\}. \tag{15}$$

The distance transform of a binary image is usually calculated considering that A_c is the set of 1-valued pixels. It results in a grayscale image, which can be naturally segmented through the watershed transform. However, it is a well known phenomenon that watersheds can lead to a severe over-segmentation and that a good selection and use of markers can prevent this.

Typical results of the distance transform calculation are illustrated in Figure 13. Four overlapping cells are shown in (a), and the binary image (b) associated to it is obtained from a first "coarse" segmentation, which is not capable of separating them. This first segmentation step can be performed through any of the standard methods according to the characteristics of the addressed problem. The image in Fig. 13(b) is negated to obtain the image in (c), the distance transform is obtained from this, and after complementing it, the resulting grayscale image is shown in (d), where the darkest points inside the cells are those farthest from the white background in (c) and appear as minima. The watershed transform is then applied using markers and minima imposition, allowing the final result shown in (e). It is worth noting that determining the markers to be used during segmentation of the aggregates using the distance and watershed transforms is not a trivial task.

The watershed method for the segmentation of aggregates is applied in [31], which used the watershed transformation for segmentation of macrophages. Another alternative is shown in [82], where the watershed transform is applied after determining markers from aggregating and overlapping templates based on some prior biological knowledge, extracted as rules or image samples. A system specifically oriented to the cytokinesis-blocked micronucleus (CBMN) test in human peripheral blood lymphocytes is presented in [83]. Here a method for detecting seed points of clumps to be used as markers was performed by alternate ultimate erosion with four- and eight-neighborhood structuring elements. Then the watershed transform was used to separate the aggregate components. The performance of the method was evaluated by splitting different clumps in CBMN images and showed better results than the traditional watershed method.
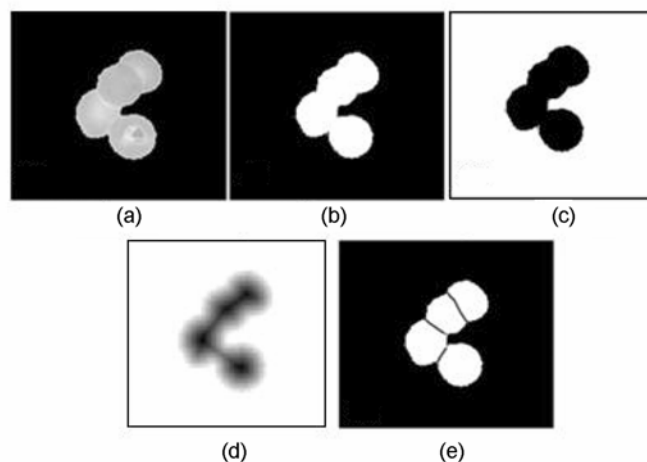

(a)   (b)   (c)

(d)   (e)

37

Fig. (13). Separating aggregates using the distance and watershed transforms, (a) original image, (b) the binary mask from a first segmentation that does not separate the aggregates, (c) complement of (b), (d) complemented distance transform of (c), and (e) final segmentation result.

A more detailed study of the use of markers in the watershed transform to split aggregates is presented in [84]. In this work, an adaptive version of the *H-minima* transform was introduced, in order to obtain extended minima of the distance map and use them as markers. The outer distance transform was also used here as a means to obtain smoother watershed lines. The algorithm was tested for neuronal and Drosophila cell images showing over 95% of clumps correctly segmented. In [85], a technique was developed, based in the analysis of the morphological scale-space generated by iterative erosion and a subsequent determination of cell-specific markers. This method is independent of the cell shapes, intensity variation inside the objects and has good convergence. The algorithm was tested using synthetic images, light microscope images of cell clusters and high resolution, transparent flat bed scanned images of stained histological sections of mouse brains, obtaining better results than the traditional watershed method when evaluated by comparison to a human-segmented ground truth.

Splitting cell aggregates in histopathological images is addressed in [86]. A binary segmentation map is obtained in which the cell nuclei and the aggregates appear as connected components separated from the other regions. These components are then classified as aggregates or single cells by smoothing out their boundaries using Fourier shape descriptors. Then an iterative splitting algorithm is applied only to the aggregates. It is based in detecting previously the most likely concave points in the connected components: the aggregate is divided in two by cutting along these points. The method was tested on 21 Follicle Lymphoma images considered as challenging, having obtained an average error rate of 5.2%.

In [87] a method to split cell aggregates based in template matching is presented. A template for a single cell is estimated by applying an expectation-maximization algorithm to a set of cells that are considered to be correctly segmented. Then the

template is iteratively matched to the areas within the aggregates, and the matched areas are removed. The algorithm was evaluated by comparing the number of cells resulting from splitting the aggregates by means of the algorithm, to the results from a human analyst, and showed agreement above 90 % for the specific images used in the experiments. In [88] an automatic method is developed for segmentation of touching cells, oriented to images from genome-wide RNAi experiments in high content screening. A scale-adaptive steerable filter is used firstly to enhance the image, for extracting long and thin protrusions on the spiky cells. The method comprises two steps, corresponding to nuclei and cytoplasm segmentation. Firstly, nuclei are extracted and labeled to initialize cytoplasm segmentation. Then initial contours of cells are found using a region growing algorithm. Secondly, a method known as graph cuts-based active contours (GCBAC) was used to segment RNAi cells using initial contours. Finally, a morphological algorithm is combined with GCBAC to separate tightly clustered cells. This method was tested by comparing the results to a manually segmented ground truth, and showed a higher precision when compared to watershed segmentation, as well as less time consumption and better efficacy than a geodesic active contour method.

An unsupervised Bayesian classification scheme is presented in [89] to separate overlapped nuclei. Here the distance map obtained by calculating the distance transform of the binary mask associated to the overlapped nuclei is considered as a mixture of Gaussians. The parametric expectation-maximization (EM) algorithm is used to learn the distribution of the topographic surface and cluster validation is performed to determine how many nuclei are overlapped. This method makes use of a priori knowledge about the regular shape of the aggregates to obtain more accurate segmentation results. The method was tested and compared to other standard methods to split cell clumps from samples of cervical cells and mammary invasive ductal carcinomas, and exhibited a better segmentation performance.

Reference [90] addresses the problem of touching cells in fluorescence microscopy in a high content screening application. The method here is based in the analysis of contours in terms of concavities and convexities, when represented as linearized lines. Special points are defined to represent convex or concave changes in the direction of

chain codes between neighboring lines and used to represent the morphological structure of the contour regions. A touching model of the clumped objects in the image is built and segmentation points are defined from the previous analysis. Finally the segmented cells are reconstructed to improve the quality of the results. An evaluation was performed using time-lapse fluorescent microscopy images of HeLa cells, with results expressed in terms of correct segmentation rate. A qualitative comparison to watershed segmentation is presented as well, showing improvements in recognition, segmentation and reconstruction of touching cells. A method based in level sets is presented in [91] applied to histopathology images. The algorithm has two steps: firstly seeds in each cell are found by a method based in single pass voting and mean-shift detection. Secondly, the segmentation is completed using level sets with a repulsion force to penalize any object overlap, in which the previously detected seeds are used

for initialization. The method's performance was evaluated in terms of precision and recall using a ground truth created by human experts created, and compared to five other algorithms showing better results. A discussion on computational efficiency is also provided, including a parallel implementation.

As can be concluded, there is not a general solution for separation of aggregates in cell images, and task specific algorithms are devised in most cases.

3.5. Evaluating the accuracy of segmentation

We have seen previously that there are numerous segmentation techniques and that so far there is not a general solution for the problem of cell segmentation. Instead, the particular characteristics of the cellular microscopy images obtained from a specific experiment are determinant in regard of what segmentation method could be the best for this case: every method has its own merits and limitations, depending upon the application. As a consequence, evaluating the effectiveness of a segmentation method for a particular task is of paramount importance. However, it is to be noticed that the problem of segmentation evaluation in cellular imaging suffers from the same drawbacks of the general problem of algorithm evaluation in image processing, such as lack of public image databases, poor information on the implementation of published algorithms, low level of standardization of the parameters to be calculated and used

when making comparisons between algorithms, and others. This problem is addressed in [92], where recommendations are issued to allow reproducibility of the experiments in the general field of signal processing. In the case under discussion here, there exist well documented supervised and non supervised methods for segmentation evaluation. In [93] a comprehensive treatment of this topic can be found.

Supervised methods use some a priori knowledge, such as a reference image or ground truth, with known results of the segmentation process. Ground truth images for segmentation evaluation usually are based in the manual segmentation of representative images made by human experts. With supervised methods, the constituent parts of the segmented images should be labeled and used for a quantitative evaluation. The performance is measured by calculating some measure of the discrepancy between the considered segmentation and the ground truth segmentation. Non supervised methods, on the other hand, are based on the computation of some statistics associated to the image.

Supervised methods are preferred whenever there is an appropriate ground truth image, for which datasets for benchmarking should be created. The use of these datasets is important because they establish references that allow the researchers to make comparisons between methods under a common framework. A general approach to the problem of creating benchmarks for segmentation evaluation is shown in [94], where a comparison is made between five different image segmentation methods, based to their ability to separate perceptually salient structures from the background, with a relatively small number of segments. However in this work the images used for benchmarking are of general nature and the results are obtained for the specific benchmarking measures introduced, therefore the importance of these results for the case of cell images is mainly methodological.

In [95], a more specific set of images for benchmarking and validation in biological image segmentation is presented. Here representative datasets of microbiological structures are provided, whose scales range from subcellular level (nm) to tissue level (μm).

There are various quantitative metrics used to evaluate the quality of segmentation algorithms. We will emphasize here those used in supervised evaluation, which is more employed in the field of interest. One of them is the Jaccard coefficient, which is a similarity measure between the ground truth and the computer-segmented objects,

$$J(A, B) = \frac{|A \cap B|}{|A \cup B|}, \qquad 0 \le J(A, B) \le 1 \, , \tag{16}$$

where $|\cdot|$ means the cardinality of the sets of pixels in the connected components that are being compared. In terms of binary images, as those resulting from a segmentation process, the Jaccard coefficient is the ratio between the numbers of pixels in the intersection and in the union, respectively, of a segmented image object A and the corresponding object B in the ground truth image, as illustrated in Figure 14. Here a value of 1 indicates a perfect coincidence between the two objects, while a value equal to zero means total absence of coincidence, practical cases being in between.
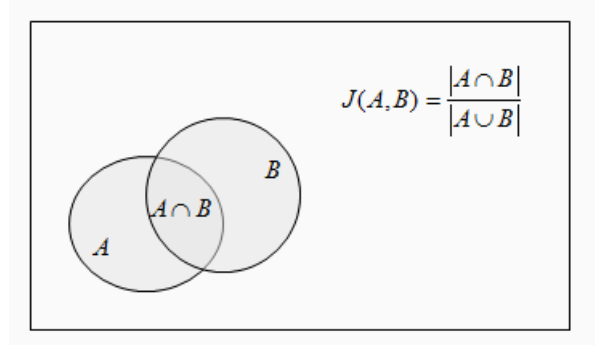

$$J(A,B) = \frac{|A \cap B|}{|A \cup B|}$$

Fig. (14). Illustration of the Jaccard coefficient calculation.

The Dice coefficient, closely related to the Jaccard coefficient, is another widely used measure, defined as

$$D(A, B) = \frac{2|A \cap B|}{|A| + |B|}, \qquad 0 \le D(A, B) \le 1 \, . \tag{17}$$

A third measure of interest is the Vinet distance [93], which gives a dissimilarity measure between two segmentation results. Let $C_1 = \{c_1^1, ..., c_{N1}^1\}$ and $C_2 = \{c_1^2, ..., c_{N2}^2\}$ be the two sets to be compared. Then a superposition table $T(C_1, C_2)$ is computed in which

$$T(C_1, C_2) = \left[|c_i^1 \cap c_j^2| \right], \qquad \begin{cases} i = 1, ..., N1 \\ j = 1, ..., N2 \end{cases} \, . \tag{18}$$

42

The components *C'* that maximize $\left|c_i^1 \cap c_j^2\right|$ are conserved and the Vinet distance is given by

$$D(C_1, C_2) = N - \sum_{C'} \left|c_i^1 \cap c_j^2\right|,$$

(19)

where *N* is the number of pixels in the segmentation result.

An example of the use of the Jaccard coefficient can be found in [94]. A method for segmentation evaluation in cell images based in the combination of region differencing with a method that allows dealing with over- and under-segmented regions is presented in [30]. Here a matrix is constructed whose elements reflects the amount of agreement between segmented and ground truth regions which takes into account the degrees of overlap and non overlap as well as the degree of uncertainties, and finally an overall similarity measure is derived. In [96] an object-level metric is presented for segmentation evaluation, devoted to measure errors due to over- and under-segmentation and penalize large deviations in the shape of segmented objects. This metric is expressed as a formula that takes into account the number of segmented regions, the size and shape of the regions of missed pixels, the size and shape of the region of excess pixels, the fraction of nuclei detected and the number of extra segmented regions. Some experiments were made using the watershed transform in order to study the relation between the segmentation quality of cell nuclei and the variations of the metric, showing good results. However this study did not include an assessment of the correlation between the metric and visual evaluation by human observers.

A valuable study from a methodological point of view, comparing nine different segmentation algorithms applied to two different cell lines and five different sets of imaging conditions, is presented in [97]. A-10 rat smooth muscle cells with some processing were used to obtain, by fluorescence microscopy, the images used in the evaluation, with manually segmented masks used as ground truth. The authors introduced a bivariate similarity index metric that evaluates the degree of under- or overestimating a cell object. This study included an analysis of the influence of cell edge sharpness on segmentation accuracy. The conclusions recognize that the performance

of segmentation algorithms depends heavily on cell morphology and imaging parameters. Reference [98] presents an evaluation of four segmentation algorithms using cumulative probability distribution functions (CDF) in order to reflect the stochastic properties of the population of misclassification errors, for quantitative descriptors of cell morphology that involve pixel counts. Fluorescence images from A10 rat smooth muscle cells and NIH-3T3 fibroblasts were used in this study at three different conditions, from which manually segmented masks were obtained as ground truth. The sum of counts of false positive and false negative pixels when comparing the segmentation results to the ground truth image is divided by the cardinality of the segmented set of pixels, to obtain the misclassification percentage for a given object. Then a study based on the CDF of these percentages for the whole population of cells is made. The comparison criterion is here that the algorithm showing uniformly the largest CDF over the entire domain of the CDF is the best one.

The human limitations to segment cell images manually has led to attempts to create simulated ground truth images, a task which can be very complex due to the huge diversity of cellular attributes like morphology, texture, etc. to be represented faithfully. An example of this can be found in [99] and [100], where basic strategies for modeling cell shapes are proposed. Here parametric models can be generated providing specific control over the simulated shapes, and leading to realistic simulations when the parameters are appropriately estimated from real data. Modifying the model's parameters allows generating cell populations with varying characteristics. Another option is learning the shapes from a set of examples. Figure 15 shows an original image and a simulated image of erythrocytes in a peripheral human blood smear, synthesized using parametric models.
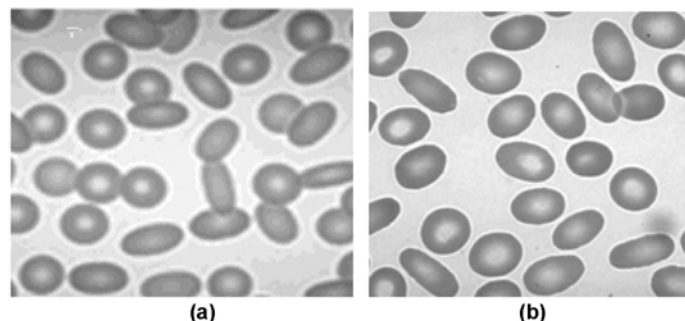

(a)   (b)

Fig. (15). Grayscale images of erythrocytes in peripheral blood smear, (a) simulated image using parametric models and (b) a real microscopy image.

Another work in which a toolbox was created to generate 3D digital phantoms of specific cellular components is reported in [101]. This system is also capable of introducing in the images the degradation due to optics and electronics. The synthetic images were tested using several similarity criteria such as visual comparison, histograms of the intensity, central moments, frequency analysis, entropy and 3D Haralick features. The simulator uses mainly geometrical concepts and can generate three different types of objects: microspheres, HL-60 cell nuclei and granulocyte nuclei.

As a last example, in [102] a general framework for estimation and simulation was created to analyze the role of fluorescence-tagged proteins moving around the Golgi apparatus and participating in the intracellular transport. The image sequences were considered as formed by two components: the static background and the tagged vesicles as moving spots with variable velocities. The former was represented by a linear model with parameters estimated from the image sequences, and the latter by a network-based dynamical model. This framework can also be applied in general problems of evaluating object detection/tracking algorithms in video-microscopy and in fluorescence time-lapse microscopy imaging, using the obtained image sequences as ground truth. The authors of this paper recommended further validations with biologist experts in order to make improvements to the system.

The simulation of realistic cell images is a real challenge due to the huge diversity of situations to be considered, however there is currently a significant activity in the field, as can be appreciated from the analyzed references.

There are three final remarks in this section: firstly, it is to be emphasized that segmentation evaluation is mandatory whenever a rigorous proof of the effectiveness of segmentation is required for a specific problem in cellular microscopy imaging. Secondly, there is currently a lack of benchmarking databases for cell image processing. Such databases have proved to be very effective in the field of general biological signal and image processing [103], allowing the comparison of results from new algorithms against those from previously developed ones, without the need of

repeating experiments. There are currently efforts to create dedicated databases for some areas in biological microscopy images [104], but there is much work to be done yet. Finally, a lack of rigorous statistical treatments in the comparison of results is observed. Using hypotheses testing would be very advisable to compare segmentation results using evaluation parameters that have inherent randomness, however this has not been usually employed in these studies.

4. FEATURE EXTRACTION AND CELL CLASSIFICATION

Automated analysis in cell imaging generally implies, after appropriate segmentation has been performed, that the regions of interest like cells, nuclei, cytoplasm or cell organelles had been isolated from the whole image and analyzed individually for purposes like anomaly detection, cell classification or pattern recognition tasks in general. These tasks are accomplished by means of computational statistical methods that are encompassed today in the field known as machine learning [105], a branch of artificial intelligence which is widely applied currently in biomedical research. In machine learning, the goal is designing algorithms capable of recognizing complex patterns in the input data and making decisions, like those associated to classification based on these data. A review on cellular image analysis and applications using these techniques is presented in [106]. A basic step in analyzing cell images is the extraction of significant features that can be used with high effectiveness for the above mentioned purposes. These features are to be selected with a task-orientation sense, because using features of low discriminating power can mean an increase of the computational load that is not rewarded in the quality of the results. The biological meaning of the features is also important to interpret the biological processes from which the images were obtained. In the case of cells, a wide variety of morphological attributes have been employed for various analysis tasks.

Some traditional features used in cell image analysis are morphometric measures taken on the segmentation mask (the binary image obtained after segmentation): area, perimeter, eccentricity (usually calculated for an ellipse having the same second moment as the region of interest), measures of convexity (convex hull, difference

between the object area and the area of its convex hull), centroid's position and minor and major axis length. Other features are measured as attributes of the segmented image in terms of mean and peak intensity, intensity variance, texture measurements, color attributes in different color spaces and others. Examples can be shown of more sophisticated or task-oriented features that have been devised for specific applications as in [107], where morphological granulometric features of nuclei were used for classification of white blood cells in bone marrow. In [108] a Scale Invariant Feature Transform (SIFT) is defined for an application in live-cell tracking. The SIFT features are extracted on the basis of successive convolutions with Gaussian functions whose results are subtracted to obtain the differences of Gaussians (DoG) in multiple scales. Finally the features are obtained as different keypoints which are identified as local extreme of the DoG images at different scales.

A last example is found in [109], which studied the cell structure and dendritic arborization from sequential optical micrographs. Some of the main features used in this work were the critical radius (radius of the circle with maximum number of intersections), the maximum number of intersections, the radial extension (distance from the cell's center to the farthest pixel of the cell skeleton), soma area and fractal dimension.

The analysis of cell images usually ends with the use of statistical modeling and classifiers, i.e. the machine learning application that was mentioned before. Different classifiers have been used in cellular image analysis, and although this topic is beyond the purposes of this review, it is worth to mention some recent examples. Support vector machines (SVM) are used for cell recognition in [110]. A neural computing system for image classification is presented in [111], this system was used to classify fluorescent stained images of lymphocytes and obtained accuracy over 85%. Another example is found in [112], where classification of boar spermatozoa in optical phase contrast images is addressed, using learning vector quantization (LVQ) to the feature vectors obtained from labeling heads as intact or damaged using stains.

5. CURRENT APPLICATIONS

We have discussed so far many works that have appeared in the scientific literature, mostly with the purpose of illustrating the image processing techniques that have been applied. However, and given that in the past decade there have been published literally hundreds of papers in the discipline of cellular image processing, a short presentation of a number of significant papers on the most recent applications can help the researchers in finding useful references for the application at hand.

Reference[128] deals with the quantification of in vivo tumor invasion and vascularization, [129] refers to application of multiple nuclei tracking to cancer cell cycle analysis, [130] is devoted to quantify cytological parameters of malignant lymphocytes, [131] treats the analysis of the population and spatial distribution of retinal ganglion cells in adult albino and pigmented mice, [132] shows a study on colon cancer cell morphology, [133] deals with 3D reconstruction of granulomas from transmitted light images, [134] is a work on automated cell detection and viability classification of suspended mammalian cells in dark field micrographs, [135] uses image processing techniques for the analysis of calcium dynamics in glial cells, [136] addresses the automated detection of mitosis in stem cell populations in phase-contrast, time-lapse microscopy to determine the time and location at which cell division is completed.

In [137] an analysis is made on computational methods and tools for automated digital reconstruction of neurons from images, oriented to the study of the structure and function of neuronal cells and networks. Reference [138] deals with the quantification of host-microbe interactions in fluorescence microscopy, [139] is on the measurement of individual red blood cell motions under high hematocrit conditions using a confocal micro-PTV system and [140] uses computer vision for automated microscopy diagnosis of malaria.

Of particular importance are the applications in high content screening. In [141] an abstract virtual instrument system is implemented using existing tools that both control the microscope and perform image analysis operations. The resulting solution is a flexible system for performing dynamic high throughput automatic microscopy. In [142] is presented a work related to hepatitis C virus replication complex, [143] is on the development of a phototransfection system as a means for performing functional

genomics manipulations on individual cells, in [144] a high content analysis method is presented for quantifying histone acetylation within a population of cells, [145] presents an approach to anti-angiogenic drug discovery, [146] shows a system for screening and pre-classification of non-organ specific auto-antibodies in diagnostics regarding systemic autoimmune and autoimmune liver diseases, and [147] treats the multidimensional quantification of subcellular morphology of Saccharomyces Cerevisiae using a specific high-throughput image-processing program. In [148] high-throughput time-lapse microscopy is used for identification and clustering of chromosome phenotypes in genome-wide RNAi screen, and [149] is devoted to the quantitative measure of alterations in the actin cytoskeleton. A segmentation method for histopathological images using color-texture information extracted by the local Fourier Transform, in an integrated framework that provides also cell clumps splitting, is presented in [86].

6. CONCLUSION

The application of Digital Image Processing in cellular imaging has received great attention in the last few years, providing new tools for improvements in biological research. The analysis of the literature reveals that there are some main problems that are to be solved in order to implement a DIP application in this field. These were identified as

- Image acquisition.
- Image restoration.
  - Correction of non uniform illumination
  - Noise filtering
  - Deblurring
- Image segmentation.
  - Application of a segmentation algorithm
  - Splitting of cell aggregates
  - Evaluation of segmentation accuracy

- Feature extraction, image analysis and classification, pattern recognition.

Image acquisition comprehends the various modalities of microscopy that can have an influence on the DIP techniques to be used. In regard to image restoration, morphological processing to correct the non uniform illumination and wavelet denoising are among the most used and successful techniques, although the use of some others have been reported in different papers with good results. Several approaches to deblurring exist that have been used in 3D fluorescence microscopy.

Denoising is an important task for which numerous filtering algorithms exist, and among them various alternatives of wavelet denoising have been used frequently in cell image processing with good results. Interpolation and super resolution techniques are potentially useful techniques due to their relationship with image resolution improvements, which is a factor to take into account in many image processing tasks. Applications of these techniques were not found in the reviewed literature.

Segmentation is an essential part of any DIP system in the field of cellular bio-imaging. There are a great number of segmentation algorithms, and adapting, combining of modifying them is usually a need when dealing with a new specific imaging problem. The most popular algorithms so far in this field have been the watershed transform and level sets, however there are many combinations and also a large number of examples in which other approaches have been used.

Splitting the cell aggregates has been an important part of the segmentation process, because in many cases the final analysis is to be carried on isolated cells. Morphological image processing and watershed methods are very important in this application.

We emphasize the need of a thorough evaluation of the performance of the segmentation algorithms, in order to decide the best choice or find the limits of accuracy of a given method. Some metrics have been developed for this purpose, and specific examples for cellular bioimaging were provided. The availability of annotated image databases that can serve as ground truth for benchmarking has been emphasized, because these allow comparing new algorithms with the existing ones without the need

of repeating experiments. However in the area of cellular bioimaging there is currently lack of such databases, for which some efforts to create them are reported.

A rigorous statistical evaluation using hypothesis testing is advisable when comparing the results of segmentation algorithms, however some lack of this kind of treatment can also be observed so far in the literature.

Feature extraction and pattern recognition appear usually in the final stages of the cellular DIP system. Applications can be very diverse, according to the specific study at hand. Among them, high content screening systems are playing currently a growing role in biological research, and a large proportion of the effort in developing new DIP systems for cellular imaging fall in this category

Given the importance acquired by biotechnology, drug development and biological research in general, as well as the huge diversity of cellular images that exist, it is to be expected that the field of DIP applications in cellular imaging will grow, with a fruitful interaction in which new algorithms developed for other applications will be introduced in this field. It is also to be expected that cellular imaging itself will pose new challenges to DIP, that will foster the development of this discipline.

Acknowledgment

References

[1] Murphy DB. Fundamentals of light microscopy and electronic imaging. New York: John Wiley & Sons; 2001.
[2] Kovacevic J, Murphy RF. Molecular and cellular bioimaging. IEEE Signal Processing Magazine 2006; 23(3):19-19.
[3] Pierzchalski A, Mittag A, Tárnok A. Observing the invisible: Molecular and cellular imaging by multimodal virtual anatomy. Cytometry Part A 2007; 71A(8): 538-39.
[4] Pierzchalski A, Robitzki A, Mittag A, Emmirch F, Sack U, O-Connor JE, Bocsi J, Tárnok A,Cytomics and nanobioengineering. Cytometry Part A 2007; 74B(6): 416-26.
[5] Attila T, Flow and image cytometry side by side for the new frontiers in quantitative single-cell analysis. Cytometry Part A 2009; 75A(3):169-71.
[6] Vonesch C, Aguet F, Vonesch J-L, Unser M. The coloured revolution of bioimaging, IEEE Signal Processing Magazine 2006; 23:20-31.
[7] Xiaobo Z, Wong, STC. Informatics challenges of high-throughput microscopy. IEEE Signal Processing Magazine 2006; 23(3): 63-72.

[8] Allalou A, Wählby C. BlobFinder, a Tool for fluorescence microscopy image cytometry. Computer Methods and Programs in Biomedicine 2009; 94(1): 58-65.

[9] Carpenter AE, Jones TR, Lamprecht MR, Clarke IHKC, Friman O, Guertin DA, Chang JH, Lindquist RA, Moffat J, Golland P, Sabatini DM. CellProfiler: image analysis software for identifying and quantifying cell phenotypes, Genome Biology 2006; 7(10): 1-11.

[10] Negishi T, Satoru N, Ohya Y. Multidimensional quantification of subcellular morphology of Saccharomyces Cerevisiae using CalMorph, the high-throughput image-processing program. Journal of Biotechnology 2009; 141(3-4): 109-17.

[11] Swedlow JR, Eliceiri KW. Open source bioimage informatics for cell biology. Trends in Cell Biology 2009; 19(11): 656-660.

[12] Chao J, Ward ES, Ober RJ. A software framework for the analysis of complex microscopy image data. IEEE Transactions on Information Technology in Biomedicine 2010; 14(4):1075-87.

[13] González RC, Woods RE. Digital image processing 3rd. ed. New Jersey: Pearson Prentice Hall; 2008.

[14] Lukak R, Plataniotis KN. Colour image processing methods and applications. Boca Raton Fla. USA: CRC Press; 2007.

[15] Yung-Sheng C (ed.). Image Processing, Vienna: InTech; 2009.

[16] Göçeri E, Loménie N. Interpolation Approaches and spline based resampling for MR images. In: Proceedings of the 2010 5th International Symposium on Health Informatics and Bioinformatics (HIBIT). 2010. pp. 137-43.

[17] Park SC, Park MK, Kang MG. Super-resolution image reconstruction: a technical overview. IEEE Signal Processing Magazine 2003; 20(3): 21-36.

[18] Akhtar P, Azhar F. A single image interpolation scheme for enhanced super resolution in bio-medical imaging. In: Proceedings of the IEEE 4th International Conference on Bioinformatics and Biomedical Engineering (iCBBE). 2010. pp. 1-5.

[19] Hiemann R, Hilger N, Sack U, Martin W. Objective quality evaluation of fluorescence images to optimize automatic image acquisition. Cytometry Part A 2006; 69A(3):182-84.

[20] Zeder M, Kohler E, Pernthaler J. Automated quality assessment of autonomously acquired microscopic images of fluorescently stained bacteria. Cytometry Part A 2010; 77A(1): 76-85.

[21] Poon SSS, Wong JT, Saunders DN, Ma QC, McKinney S, Fee SJ, Aparicio AJR. Intensity calibration and automated cell cycle gating for high-throughput image-based siRNA screens of mammalian cells. Cytometry Part A 2009; 73A(10): 904-17.

[22] Syed TQ, Vigneron V, Lelandais S, Barlovatz-Meimon G, Malo M, Charriere-Bertrand C, Montagne C. Detection and counting of "in vivo" cells to predict cell migratory potential. In: Proceedings of the IEEE First Workshops on Image Processing Theory, Tools and Applications, IPTA'08. 2008. pp. 24-26.

[23] Sysko LR, Davis MA. From image to data using common image-processing techniques. Current Protocols in Cytometry 2010; Published online in Wiley Online Library (wileyonlinelibrary.com), pp. 12.21.1-12.21.17.

[24] Soille P. Morphological image analysis. Berlin: Springer Verlag; 2003.

[25] Selvaggio G, Ceroni F, Giordano E, Lorenzo-Ginori JV. Evaluation of the expression level of a fluorescent protein in single cells through digital image processing. IFMBE Proceedings 2011; 33:.

[26] Jiménez-Sánchez AR, Mendiola-Santibañez JD, Terol-Villalobos IR, Herrera-Ruíz G, Vargas-Vázquez D, García-Escalante JJ, et al. Morphological background detection and enhancement of images with poor lighting. IEEE Transactions on Image Processing 2009; 18(3): 613-23.

[27] Matula P, Kumar A, Wörz I, Erfle H, Bartenschlager R, Eils R, Rohr K. Single-cell based image analysis of high-throughput cell array screens for quantification of viral infection. Cytometry Part A 2009; 75A(4): 309-18.

[28] Osman MK, Mashor MY, Saad Z, Jaafar H. Colour image segmentation of tuberculosis bacilli in Ziehl-Neelsen-stained tissue images using moving k-mean clustering procedure. In: Proceedings of the Fourth Asia International Conference on Mathematical/Analytical Modelling and Computer Simulation (AMS). 2010. p. 215-20. .

[29] Wei D-Y, Yin C-C. An optimized locally adaptive non-local means denoising filter for cryo-electron microscopy data. Journal of Structural Biology 2010; 172(3): 211-18.

[30] Hodneland E, Bukoreshtliev NV, Eichler TW, Tai X-C, Gurke S, Lundervold A, et al. A unified framework for automated 3-D segmentation of surface-stained living cells and a comprehensive segmentation evaluation. IEEE Transactions on Medical Imaging 2009; 28(5): 720-738.

[31] Ruihua X, Ping W, Guo F. One kind of macrophages images segmentation and labeling method. In: IEEE 2nd International Congress on Image and Signal Processing, CISP '09. 2009. p. 1-5.

[32] Walter T, Held M, Neumann B, Hériché J-K, Conrad C, Pepperkok R, et al. Automatic identification and clustering of chromosome phenotypes in a genome wide RNAi screen by time-lapse imaging. Journal of Structural Biology 2010; 170(1):1-9.

[33] Boulanger J, Kervrann C, Bouthemy P, Elbau P, Sibarita JB, Salamero J. Patch-based nonlocal functional for denoising fluorescence microscopy image sequences. IEEE Transactions on Medical Imaging 2010; 29(2): 442-54.

[34] Rodrigues, IC, Sanches JMR. Convex total variation denoising of Poisson fluorescence confocal images with anisotropic filtering. IEEE Transactions on Image Processing 2011; 20(1): 146-160.

[35] Bo Z, Fadili JM, Starck JL. Wavelets, ridgelets, and curvelets for Poisson noise removal. IEEE Transactions on Image Processing 2008; 17(7): 1093-1108.

[36] Szabó LZ, Vincze J, Csernoch L, Szentesi P. Improved spark and ember detection using stationary wavelet transforms. Journal of Theoretical Biology 2010; 264(4): 1279-92.

[37] Luisier F, Vonesch C, Blu T, Unser M. Fast Haar-wavelet denoising of multidimensional fluorescence microscopy data. In: Proceedings of the IEEE International Symposium Biomedical Imaging: From Nano to Macro, ISBI'09. 2009. p. 310-13.

[38] Padfield D, Rittscher J, Roysam B. Coupled minimum-cost flow cell tracking for high-throughput quantitative analysis. Medical Image Analysis 2011; 15:650-88.

[39] Sarder P, Nehorai A. Deconvolution methods for 3-D fluorescence microscopy images. IEEE Signal Processing Magazine 2006; 23(3): 32-45.

[40] Ramani S, Vonesch C, Unser M, Deconvolution of 3D fluorescence micrographs with automatic risk minimization. In: Proceedings of the 5th IEEE International Symposium on Biomedical Imaging: From Nano to Macro, ISBI'08. 2008. p. 732-35. .

[41] Aguet F, Van De Ville D, Unser M. Model-based 2.5-d deconvolution for extended depth of field in brightfield microscopy. IEEE Transactions on Image Processing 2008; 17(7): 1144-53.

[42] Abraham T, Allan SE, Levins MK, Deconvolution and chromatic aberration corrections in quantifying colocalization of a transcription factor in three-dimensional cellular space. Micron 2010; 41(6): 633-40.

[43] Bayram I, Guerquin-Kern M, Terrés-Kristofani R, Unser M, Accelerated wavelet-regularized deconvolution for 3-D fluorescence microcopy. In: Proceedings of the 17th IEEE International Conference on Image Processing ICIP'2010. 2010. p. 581-84.

[44] Kenig T, Kam Z, Feuer A. Blind image deconvolution using machine learning for three-dimensional microscopy. IEEE Transactions on Pattern Analysis and Machine Intelligence 2010; 32(12): 2191-204.

[45] Meijering E. Cell Segmentation: 50 Years Down the Road. IEEE Signal Processing Magazine 2012; 29(5): 140-145.

[46] Angulo J, Schaack B.Morphological-based adaptive segmentation and quantification of cell assays in high content screening. In: Proceedings of the 5th IEEE International Symposium on Biomedical Imaging: From Nano to Macro ISBI'08. 2008. p. 360-63.

[47] Lin G, Chawla MK, Olson K, Barnes CA, Guzowski JF, Bjornsson C, et al. A multi-model approach to simultaneous segmentation and classification of heterogeneous populations of cell nuclei in 3D confocal microscope images. Cytometry Part A 2007; 71A(9): 724-36.

[48] Marcuzzo M, Quelhas P, Campilho A, Mendonça AM, Campilho A. Automated Arabidopsis plant root cell segmentation based on SVM classification and region merging. Computers in Biology and Medicine 2009; 39(9): 785-93.

[49] Mashburn DN, Lynch HE, Ma X, Hutson MS. Enabling User-Guided segmentation and tracking of surface-labeled cells in time-lapse image sets of living tissues. Cytometry Part A 2011; 81A(5): 409-18.

[50] Osher SS, Sethian J. Fronts propagating with curvature dependent speed: Algorithms based on Hamilton-Jacobi formulations. Journal of Computational Physics 1988; 79:12-49.

[51] Bazán C, Miller M, Blomgrem P, Structure enhancement diffusion and contour extraction for electron tomography of mitochondria, Journal of Structural Biology 2009; 166(2): 144-55.

[52] Dzyubachyk O, Van Cappellen WA, Essers J, Niessen WJ, Meijering E. Advanced level-set-based cell tracking in time-lapse fluorescence microscopy. IEEE Transactions on Medical Imaging 2010; 29(3): 852-67.

[53] Huiming P, Xiaobo Z, Li F, Xia X, Wong S.T.C. Integrating multi-scale blob/curvilinear detector techniques and multi-level sets for automated segmentation of stem cell images. In: Proceedings of the IEEE International Symposium on Biomedical Imaging: From Nano to Macro ISBI'09. 2009. p. 1362-65**.**

[54] Padfield D, Rittscher J, Thomas N, Roysam B. Spatio-temporal cell cycle phase analysis using level sets and fast marching methods. Medical Image Analysis 2009; 13(1): 143-55.

[55] Weimiao Y, Lee HK, Hariharan S, Wenyu B, Ahmed S. Quantitative neurite outgrowth measurement based on image segmentation with topological dependence. Cytometry Part A 2009; 75A(4): 289-97.

[56] Srinivasa G, Fickus MC, Guo Y, Linstedt AD, Kovačević J. Active mask segmentation of fluorescence microscope images. IEEE Transactions on Image Processing 2009; 18(8):1817-29.

[57] Spetsieris K, Zygourakis K, Mantzaris NV. A novel assay based on fluorescence microscopy and image processing for determining phenotypic distributions of rod-shaped bacteria. Biotechnology and Bioengineering 2009; 102:598-615.

[58] Quelhas P, Marcuzzo M, Mendonça AM, Campilho A. Cell nuclei and cytoplasm joint segmentation using the sliding band filter. IEEE Transactions on Medical Imaging 2010; 29(8): 1463-73.

[59] Chen P, Huijuan L, Feilong C. Segmentation of blood and bone marrow cell images via learning by sampling, Lecture Notes in Computer Science 2009; 5754:336-45.

[60] Comaniciu D, Meer P. Mean-shift: a robust approach toward feature space analysis, IEEE Transactions on Pattern Recognition and Machine Intelligence 2002; 24(5):603-19.

[61] Guo N, Zeng L, Wu Q. A method based on multispectral imaging technique for white blood cell segmentation, Computers in Biology and Medicine 2007; 37(1): 70-6.

[62] Bell A, Herberich G, Meyer-Ebrecht D, Böcking A, Aach T. Segmentation and detection of nuclei in silver stained cell specimens for early cancer diagnosis. In: Proceedings of the IEEE International Conference on Image Processing. 2007. p. VI-49 - VI-52.

[63] Mao KZ, Peng Z, Tan P-H. Supervised learning-based cell image segmentation for P53 immunohistochemistry, IEEE Transactions on Biomedical Engineering 2006; 53(6): 1153-63.

[64] Di Cataldo S, Ficarra E, Aquaviva A, Macii E. Automated segmentation of tissue images for computerized IHC analysis, Computer Methods and Programs in Biomedicine 2010; 100(1): 1-15.

[65] Wu H-S, File M, Schiano TD, Gil J. Image segmentation of liver fibrosis. Journal of Microscopy 2008; 231(1): 70–80.

[66] Gudla PR, Nandy K, Collins J, Meaburn KJ, Misteli T, Lockett SJ. A high-throughput system for segmenting nuclei using multiscale techniques. Cytometry Part A 2008; 73A(5): 451-66.

[67] Ko BC, Seo MS, Nam J-Y. Microscopic cell nuclei segmentation based on adaptive attention window. Journal of Digital Imaging 2009; 22(3): 259-74.

[68] Fenistein D, Lenseigne B, Christophe T, Brodin P, Genovesio A. A fast, fully automated cell segmentation algorithm for high-throughput and high-content screening. Cytometry Part A 2008; 73A(10):958-64.

[69] Xiaobo Z, Fuhai L, Yan J, Wong STC. A novel cell segmentation method and cell phase identification using Markov model. IEEE Transactions on Information Technology in Biomedicine 2009; 13(2): 152-7.

[70] Bergen T, Steckhan D, Wittenberg T, Zerfaß T. Segmentation of leukocytes and erythrocytes in blood smear images. In: Proceedings of the IEEE 30th Annual International Conference of the Engineering in Medicine and Biology Society EMBS. 2008. p. 3075-78.

[71] Bradhurst CJ, Boles W, Xiao Y. Segmentation of bone marrow stromal cells in phase contrast microscopy images. In: Proceedings of the IEEE 23rd International Conference on Image and Vision Computing New Zealand IVCNZ. 2008. p. 1-6.

[72] Calapez A, Rosa A. A statistical pixel intensity model for segmentation of confocal laser scanning microscopy images. IEEE Transactions on Image Processing 2010; 19(9):2408-.18.

[73] Korzynska A., Strojny W, Hoppe A, Wertheim D, Hoser P. Segmentation of microscope images of living cells. Pattern Analysis & Applications 2007; 10(4):301-19.

[74] McCullough DP, Gudla PR, Harris BS, Collins JA, Meaburn KJ, Nakaya M-A, et al. Segmentation of whole cells and cell nuclei from 3-D optical microscope images using dynamic programming. IEEE Transactions on Medical Imaging 2008; 27(5): 723-34.

[75] Russell RA, Adams NM, Stephens DA, Batty E, Jensen K, Freemont PS. Segmentation of fluorescence microscopy images for quantitative analysis of cell nuclear architecture. Biophysical Journal 2009; 96(8): 3379-89.

[76] Vermolen B, Garini Y, Young IT, Dirks RW, Raz V. Segmentation and analysis of the three-dimensional redistribution of nuclear components in human mesenchymal stem cells, Cytometry Part A 2008; 73A(9):816-24.

[77] Sobrevilla P, Montseny E, Vaschetto F, Lerma E. Fuzzy-based analysis of microscopic colour cervical pap smear images: nuclei detection. International Journal of Computational Intelligence and Applications 2010; 9(3):187-206.

[78] Gençtav A, Aksoy S, Önder S. Unsupervised segmentation and classification of cervical cell images. Pattern Recognition 2012; 45(12): 4151-68.

[79] Ficarra E, Di Cataldo S, Acquaviva A. Macii E. Automated Segmentation of Cells With IHC Membrane Staining. IEEE Transactions on Biomedical Engineering 2011; 58(5): 1421-29.

[80] Korzyńska A, Iwanowski M. Multistage morphological segmentation of bright-field and fluorescent microscopy images. Opto-Electronics Review 2012; 20(2): 174-86.

[81] Al-Kofahi Y, Lassoued W, Roysam B. Improved Automatic Detection and Segmentation of Cell Nuclei in Histopathology Images. IEEE Transactions on Biomedical Engineering 2010; 57(4): 841-52.

[82] Cloppet F, Boucher A. Segmentation of overlapping/ aggregating nuclei cells in biological images. In: Proceedings of the 19th International Conference on Pattern Recognition ICPR 2008. 2008. p. 1-4.

[83] Yan XK, Zhang N, Chen Y, Du J, Cao Z-S, Zhou P-K. Splitting of cell clumps in cytokinesis-blocked micronucleus images: Application to improve the recognition ability of binucleated lymphocytes, Cytometry Part A 2010; 77A(8):783-89.

[84] Jierong C, Rajapakse JC. Segmentation of clustered nuclei with shape markers and marking function. IEEE Transactions on Biomedical Engineering 2009; 56(3): 741-48.

[85] Schmitt O, Hasse M. Morphological multiscale decomposition of connected regions with emphasis on cell clusters. Computer Vision and Image Understanding 2009, 113(2):188-201.

[86] Kong H, Gurcan M, Belkacem-Boussaid K. Partitioning histopathological images: An integrated framework for supervised colour-texture segmentation and cell splitting. IEEE Transactions on Medical Imaging 2011; 30(9): 1661-7.

[87] Diaz G, Gonzalez F, Romero E. Automatic clump splitting for cell quantification in microscopic images, Lecture Notes in Computer Science 2008; 4756: 763-72.

[88] Chen C, Li H, Zhou X, Wong STC. Constraint factor graph cut-based active contour method for automated cellular image segmentation in RNAi screening. Journal of Microscopy 2008; 230(2): 177-91.

[89] Chanho J, Changick K, Seoung WC, Sukjoong O, Unsupervised segmentation of overlapped nuclei using Bayesian classification. IEEE Transactions on Biomedical Engineering 2010; 57(12): 2825-32.

[90] Donggang Y, Pham TD, Zhou X. Analysis and recognition of touching cell images based on morphological structures. Computers in Biology and Medicine 2009; 39(1): 27 – 39.

[91] Qi X, Xing F, Foran DJ, Yang L. Robust segmentation of overlapping cells in histopathology specimens using parallel seed detection and repulsive jevel set. IEEE Transactions on Biomedical Engineering 2012; 59(3): 754-65.

[92] Vandewalle P, Kovačević J, Vetterli M. Reproducible Research in Signal Processing. IEEE Signal Processing Magazine 2009; 26(3): 37-47.

[93] Rosenberger C, Chabrier S, Laurent H, Emile B. Unsupervised and supervised image segmentation evaluation. In: P Y-J Zhang, editor. Advances in Image and Video Segmentation, Beijing: Idea Group Inc; 2005, p. 365-93.

[94] Feng G, Wang S, Liu T. A new benchmark for image segmentation evaluation. Journal of Electronic Imaging 2007; 16(3): 033011-6.

[95] Gelasca ED, Jiyun B, Obara B, Manjunath BS Evaluation and benchmark for biological image segmentation. In: Proceedings of the 15th IEEE International Conference on Image Processing, ICIP'2008. 2008. p. 1816-19.

[96] Boucheron LE, Harvey NR, Manjunath BS. A Quantitative object-level metric for segmentation performance and its application to cell nuclei. Advances in Visual Computing, Lecture Notes in Computer Science 2007; 4841: 208-19.

[97] Dima AA, Elliott JT, Filliben JJ, Halter M, Peskin A, Bernal J, et al. Comparison of segmentation algorithms for fluorescence microscopy images of cells. Cytometry Part A 2011; 79A(7): 545-59.

[98] Hagwood C, Bernal J, Halter M, Elliott J. Evaluation of segmentation algorithms on cell populations using CDF curves. IEEE Transactions on Medical Imaging 2012; 31(2): 380-90.

[99]   Lehmussola A, Ruusuvuori P, Selinummi J, Huttunen H, Yli-Harja O. Computational framework for simulating fluorescence microscope images with cell populations. IEEE Transactions on Medical Imaging 2007. 26:1010-.16.

[100] Lehmussola A, Ruusuvuori P, Selinummi J, Rajala T, Yli-Harja O. Synthetic images of high-throughput microscopy for validation of image analysis methods. Proceedings of the IEEE 2008; 96(8):1348-60.

[101] Svoboda D, Kozubek M, Stejskal S. Generation of digital phantoms of cell nuclei and simulation of image formation in 3D image cytometry. Cytometry Part A 2009; 75A(6): 494-509.

[102] Boulanger J, Kervrann C, Bouthemy P. A simulation and estimation framework for intracellular dynamics and trafficking in video-microscopy and fluorescence imagery. Medical Image Analysis 2009; 13(1): 132-42.

[103]   Physionet. Available from http://www.physionet.org,

[104]   Bisque bioimage database infrastructure, Center for Bio-Image Informatics, UCSB. Available from http://dough.ece.ucsb.edu,

[105] Wernick M, Yongyi Y, Brankov JG, Yourganov G, Strother SC. Machine learning in medical imaging. IEEE Signal Processing Magazine 2010; 27(4):25-38.

[106] Rittscher J. Characterization of biological processes through automated image analysis. Annual Reviews in Biomedical Engineering 2010; 12: 315-44.

[107] Theera-Umpon N, Dhompongsa S. Morphological granulometric features of nucleus in automatic bone marrow white blood cell classification. IEEE Transactions on Information Technology in Biomedicine 2007; 11(3): 353-9.

[108] Jiang RM, Crookes D, Luo N, Davidson MW. Live-cell tracking using SIFT features in DIC microscopic videos. IEEE Transactions on Biomedical Engineering 2010; 57(9): 2219-28.

[109]   Bicelli L, Pioggia G, Vaglini F, Ahluwalia A. Automated extraction and classification of dynamic metrical features of morphological development in dissociated Purkinje neurons. Journal of Neuroscience Methods 2010; 185(2): 315-24

[110]   Osowski S, Siroic R, Markiewicz T, Siwek K. Application of support vector machine and genetic algorithm for improved blood cell recognition. IEEE Transactions on Instrumentation and Measurement 2009; 58(7): 2159-68.

[111]   O'Connor MF, Hughes A, Chaoxin Z, Davies A, Kelleher D, Ahmad K. Annotation and retrieval of cell images. Lecture Notes in Computer Science 2010; 6283: 218-25.

[112]   Alegre E, Biehl M, Petkov N, Sánchez L. Automatic classification of the acrosome status of boar spermatozoa using digital image processing and LVQ, Computers in Biology and Medicine 2008; 38(4):461-68.

[113]   Krishnan MRK, Chakraborty C, Paul RR, Ray AK. Hybrid segmentation, characterization and classification of basal cell nuclei from histopathological images of normal oral mucosa and oral submucous fibrosis. Expert Systems with Applications 2012; 39(1): 1062-1077.

[114]   Phinyomark A, Jitaree S, Phukpattaranont P, Boonyapiphat P. Texture analysis of breast cancer cells in microscopic images using critical exponent analysis method. Procedia Engineering 2012; 32(0): 232-38.

[115]   Scholtens TM, Schreuder F, Ligthart ST, Swennenhuis JF, Greve J, Terstappen LWMM. Automated identification of circulating tumor cells by image cytometry 2012; Cytometry Part A 81A(2): 138-48.

[116]   Li K, Lu Z, Liu W, Yin J. Cytoplasm and nucleus segmentation in cervical smear images using radiating GVF snake. Pattern Recognition 2012; 45(4): 1255-64.

[117]   Liu A-A, Li K, Kanade T. A semi-Markov model for mitosis segmentation in time-lapse phase contrast microscopy image sequences of stem cell populations. IEEE Transactions on Medical Imaging 2012; 31(2): 359-369.

[118]   Kawaguchi H, Masamoto K, Ito H, Kanno I. Image-based vessel-by-vessel analysis for red blood cell and plasma dynamics with automatic segmentation. Microvascular Research 2012; 84(2): 178-87.

[119]   Wu X, Amrikachi M, Shah SK. Embedding topic discovery in conditional random fields model for segmenting nuclei using multispectral data. IEEE Transactions on Biomedical Engineering 2012; 59(6): 1539-49.

[120]   Kim K-M, Kim S-Y, Minxhaa J, Tayhas, Palmorea R. A novel method for analyzing images of live nerve cells. Journal of Neuroscience Methods 2011; 201(1): 98-105.

[121] Bergmeir C, García-Silvente M, Benítez JM. Segmentation of cervical cell nuclei in high-resolution microscopic images: A new algorithm and a web-based software framework. Computer Methods and Programs in Biomedicine 2012; 107(3): 497-512.

[122] Ko BC, Gim JW, Nam JY. Cell image classification based on ensemble features and random forest. Electronics Letters 2011; 47(11): 638-39.

[123] Perera PN, Schmidt M, Schuck PJ, Adams PD. Blind image analysis for the compositional and structural characterization of plant cell walls. Analytica Chimica Acta 2011; 702(2): 172-77.

[124] Plissiti ME, Nikou C, Charchanti A. Combining shape, texture and intensity features for cell nuclei extraction in Pap smear images. Pattern Recognition Letters 2011; 32(6): 838-53.

[125] Plissiti ME, Nikou C, Charchanti A. Automated Detection of Cell Nuclei in Pap Smear Images Using Morphological Reconstruction and Clustering. IEEE Transactions on Information Technology in Biomedicine 2011; 15(2): 233-41.

[126] Wu HS, Fiel MI, Schiano TD, Ramer M, Burstein D, Gil J. Segmentation of textured cell images based on frequency analysis. IET Image Processing 2011; 5(2): 148-58.

[127] Wu X, Amrikachi M, Shah SK."Embedding topic discovery in conditional random fields model for segmenting nuclei using multispectral data." IEEE Transactions on Biomedical Engineering 2012;.59(6): 1539-49.

[128] Blacher S, Jost M, Melen-Lamalle L, Lund LR, Romer J, Foidart JM. A Noël, Quantification of in vivo tumor invasion and vascularization by computerized image analysis, Microvascular Research 2008; 75(2):169-78.

[129] Fuhai L, Xiaobo Z, Wong STC. Multiple nuclei tracking using integer programming for quantitative cancer cell cycle analysis. IEEE Transactions on Medical Imaging 2010; 29(1): 96-105.

[130] Jahanmehr SAH, Rogers M, Zheng J, Lai R, Wang C. Quantitation of cytological parameters of malignant lymphocytes using computerized image analysis. International Journal of Laboratory Hematology 2008; 30: 278-85.

[131] Salinas-Navarro M, Jiménez-López M, Valiente-Soriano MJ, Alarcón-Martínez M, Avilés-Trigueros M, Mayor S, et al. Retinal ganglion cell population in adult albino and pigmented mice: A computerized analysis of the entire population and its spatial distribution, Vision Research 2009; 49(6): 637-47.

[132] Venkatesan P, Das S, Krishnan MMR, Chakraborty C, Chaudhury K, Mandal M. Effect of AEE788 and/or Celecoxib on colon cancer cell morphology using advanced microscopic techniques. Micron 2010; 41(3):247-56.

[133] Delaby A, Espinosa L, Lépolard C, Capo C, Mège J-L. 3D reconstruction of granulomas from transmitted light images implemented for long-time microscope applications, Journal of Immunological Methods 2010; 360(1-2):10-19.

[134] Burgemeister S, Nattkemper TW, Noll T, Hoffrogge R, Flaschel E. CellViCAM--Cell viability classification for animal cell cultures using dark field micrographs. Journal of Biotechnology 2010, 149(4): 310-16.

[135] Fanelli A, Titapiccolo JI, Esposti F, Ripamonti M, Malgaroli A, Signorini MG. Novel image processing methods for the analysis of calcium dynamics in glial cells. IEEE Transactions on Biomedical Engineering 2011; 58(9): 2640-7.

[136] Seungil H, Ker DFE, Bise R, Chen M, Kanade T. Automated mitosis detection of stem cell populations in phase-contrast microscopy Images. IEEE Transactions on Medical Imaging 2011; 30(3): 586-96.

[137] Meijering E. Neuron tracing in perspective. Cytometry Part A 2010; 77A(7): 693-704.

[138] Haghighat A-C, Seveau S. Quantification of host-microbe interactions by automated fluorescence microscopy. Journal of Immunological Methods 2010; 352(1-2): 186-91.

[139] Lima R, Ishikawa T, Imai Y, Takeda M, Wada S, Yamaguchi T. Measurement of individual red blood cell motions under high hematocrit conditions using a confocal micro-PTV system. Annals of Biomedical Engineering 2009; 37(8): 1546-59.

[140] Tek FB, Dempster AG, Kale I. Computer vision for microscopy diagnosis of malaria. Malaria Journal 2009, 8(53):1-14.

[141] Russel ABM, Abramson D, Bethwaite B, Dinh MN, Enticott C, Firth S, et al. An abstract virtual instrument system for high throughput automatic microscopy. Procedia Computer Science 2010; 1(1): 545-54.

[142]   Berke JM, Fenistein D, Pauwels F, Bobbaers R, Lenz O, Lin T-I, et al. Development of a high-content screening assay to identify compounds interfering with the formation of the hepatitis C virus replication complex. Journal of Virological Methods 2010, 165(2): 268-76.

[143]   Cappelleri DJ, Halasz A, Sul J-Y, Kim TK, Eberwine J, Kumar V. Toward a fully automated high-throughput phototransfection system. Journal of the Association for Laboratory Automation 2010; 15(4): 329-41.

[144]   Narayan PJ, Dragunow M. High content analysis of histone acetylation in human cells and tissues. Journal of Neuroscience Methods 2010; 193(1): 54-61.

[145]   Evensen L, Micklem DR, Link W, Lorens JB. A novel imaging-based high-throughput screening approach to anti-angiogenic drug discovery. CytometryPart A 2010; 77A(1): 41-51.

[146]   Hiemann R, Büttner T, Krieger T, Roggenbuck D, Sack U, Conrad K. Challenges of automated screening and differentiation of non-organ specific autoantibodies on HEp-2 cells. Autoimmunity Reviews 2009; 9(1): 17-22.

[147]   Negishi T, Nogami S, Ohya Y. Multidimensional quantification of subcellular morphology of Saccharomyces Cerevisiae using CalMorph, the high-throughput image-processing program. Journal of Biotechnology 2009; 141(3-4): 109-17.

[148]   Walter T, Held M, Neumann B, Hériché J-K, Conrad C, Pepperkok R, et al. Automatic identification and clustering of chromosome phenotypes in a genome wide RNAi screen by time-lapse imaging. Journal of Structural Biology 2010; 170(1): 1-9.

[149]   Weichsel J, Herold N, Lehmann MJ, Kräusslich H-G, Schwarz US. A quantitative measure for alterations in the actin cytoskeleton investigated with automated high-throughput microscopy. Cytometry Part A 2010; 77A(1): 52-63.

[150]   Lorenzo-Ginori JV. A method to determine the size of the structuring element in morphological correction of non-uniform illumination. Proceedings of the 18th IEEE International Conference on Image Processing, ICIP'2011. (2011). p. 1485-8.

De los autores:

Centro de Estudios de Electrónica y Tecnologías de la Información, Facultad de Ingeniería Eléctrica, Universidad Central "Marta Abreu" de Las Villas, Carretera a Camajuaní Km. 5 ½, 54830 Santa Clara, Villa Clara, Cuba.